AN ABSTRACT OF THE THESIS OF

Wen-Chyi Su for the degree of Master of Science in Civil Engineering presented on November 30, 1994. Title : Dynamic Response of Flexible Rotating Machine Subjected to Ground Motions.

Abstract approved : _____

Alan G. Hernried

Rotating machine play an important role in modern technology. Compressors in ventilating and cooling systems, pumps in power generation facilities, as well as high speed computer are all examples of flexible rotating machinery that must remain functional during and after a sever earthquake. Recent earthquakes have demonstrated that an aseismically designed structure may perform well during a strong earthquake yet still become nonfunctional due to damage in critical nonstructural components. For example, evacuation of several hospitals during the recent Northridge earthquake in the LA area was not caused by structural failure bur resulted from mechanical failure of the systems described above. Rotating machines are key components of such system. Further study into the behavior of these systems and technique for their protection for their protection during severe ground motion is needed.

The flexible rotating machine is significantly complex, even for highly simplified models, due to gyroscopic and other effects. This paper presents the coupled, linear partial differential equations of motion of a flexible rotating shaft subjected to ground motion. Classical and finite element methods are developed to solve these equations. The effects of various physical parameters on the response of the system; magnitude, duration, and frequency content of the ground motion; bearing stiffness and damping; flexibility of the deformation and rotatory inertia effects are investigated, Both vertical and horizontal ground motion, individually and in combination, will be considered.

Dynamic Response of Flexible Rotating Machines Subjected to Ground Motions

by

Wen-Chyi Su

A THESIS

submitted to

Oregon State University

in partial fulfillment of
the requirements for the

degree of

Master of Science

Completed November 30, 1994

Commencement June 1995

Master of Science thesis of Wen-Chyi Su presented on November 30, 1994

APPROVED :

Redacted for Privacy

Major Professor, representing Civil Engineering

Redacted for Privacy

Chair of Department of Civil Engineering

Redacted for Privacy

Dean of Graduate School

I understand that my thesis will become part of the permanent collection of Oregon State University libraries. My signature below authorizes release of my thesis to any reader upon request.

Redacted for Privacy

Wen-Chyi Su, Author

Acknowledgement

The authors are grateful to professor C. Smith of Oregon State University for his insightful discussions on rotor dynamics. The financial support of the US National Science Foundation under Grant No. CMS - 9301464 is gratefully acknowledged.

TABLE OF CONTENTS

LIST OF FIGURES

LIST OF TABLES

Dynamic Response of Flexible Rotating Machine Subjected to Ground Motions

Chapter I

Introduction and Background

I. 1 Introduction

Rotating machines play an important role in modern technology. Turbines in power plants, compressors in ventilating and cooling systems are a few examples. Since rotating machines may serve a critical function, they must be designed to withstand the potentially damaging effects of a strong earthquake.

The purpose of this study, therefore, is to present a methodology for predicting the response of a flexible rotating machine subjected to strong ground motions. The methodology will be used to determine the effects of the ground motion (duration, magnitude and frequency), speed of rotation, shaft flexibility, and bearing properties (damping and stiffness) on the response of the rotating machine. This information should then prove useful in the aseismic design of rotating machines.

I. 2 Previous research

In the past, several investigators have developed rotor models to determine the response of rotating machines subjected to seismic ground motions. To reduce the complexity of the analysis, these scientists [1-7] have ignored the flexibility of the shaft in order to specifically evaluate the effect of earthquake excitations on rotor bearings.

Some more realistic models of rotors where flexibility of the shaft is considered

have been developed. The flexible shaft has been modeled as either a Euler-Bernoulli [8] or Timoshenko [9-13] beam. The gyroscopic effects and the influence of bearing flexibility and damping on the seismic response of rotor were considered in these studies.

A rotor-bearing system model of increasing generality and complexity has been considered by Srinivasan and Soni [14,15]. A very general description of the base excitation with three translational and three rotational components was considered. Their analytical model includes the effects of rotatory inertia, shear deformation effects in the flexible shaft, and rotor-bearing interaction. Gyroscopic effects and parametric terms caused by the rotation of the base are included in the formulation. A finite element formulation of the shaft with linear interpolation functions was used to analyze the response of the rotor.

Although the finite element method with linear interpolation functions may be advantageous in some situations [15], it has been shown that such a formulation may not accurately predict some important dynamic characteristics such as instability of the rotating system [16].

Suarez, Singh and Rohanimanesh [16] extended the work of Srinivasan and Soni by using both linear as well as non-linear interpolation functions. They also showed that several velocity dependent forcing function terms were missing from the equations of motion developed by Srinivasan and Soni. New numerical results for the critical speed of rotation (the speed above which the shaft system becomes unstable) are presented. The seismic response characteristics of a rotating machine subjected to simulated base excitation are also investigated. The numerical studies indicate that the non-linear

parametric terms in the equations of motion can be ignored when the rotational base excitations are insignificant in comparison to the translational base ground motions.

I. 3 Scope

In the rotor-disk-bearing system to be considered; the model of Suarez, Singh and Rohanimanesh [16] will be used. Shear deformation effects are initially neglected in the shaft flexibility. The shaft rotates with a constant speed and may have varying properties along the length. To obtain the complete response of the rotor-bearing system, the influences of the stiffness and damping of the fluid-bearing system are also considered. It has been shown [16] that even for strong rotational inputs the parametric terms in the equations of the motion can be ignored without affecting the response; therefore, only three translation components of the ground motion are considered. The model of the rotating machine subjected to earthquake ground motions is shown in Figure 1.

In chapter two, the equations of motion for the flexible rotating shaft ignoring shear deformations are developed by a Newtonian approach and the theory of classical dynamics. In chapter three, the equations of motion for the flexible rotating shaft ignoring shear deformations are developed using energy principles and the shaft is modeled using the finite element method. The equations of the equivalent discrete parameter model are obtained using the system Lagrangian. In addition, the method of superposition [17] for including shear effects in the system is also presented in this chapter. In chapter four, the eigenvalue problem associated with the homogeneous equations of motion of the rotor-disk-bearing system will be developed and used to predict the stability characteristics

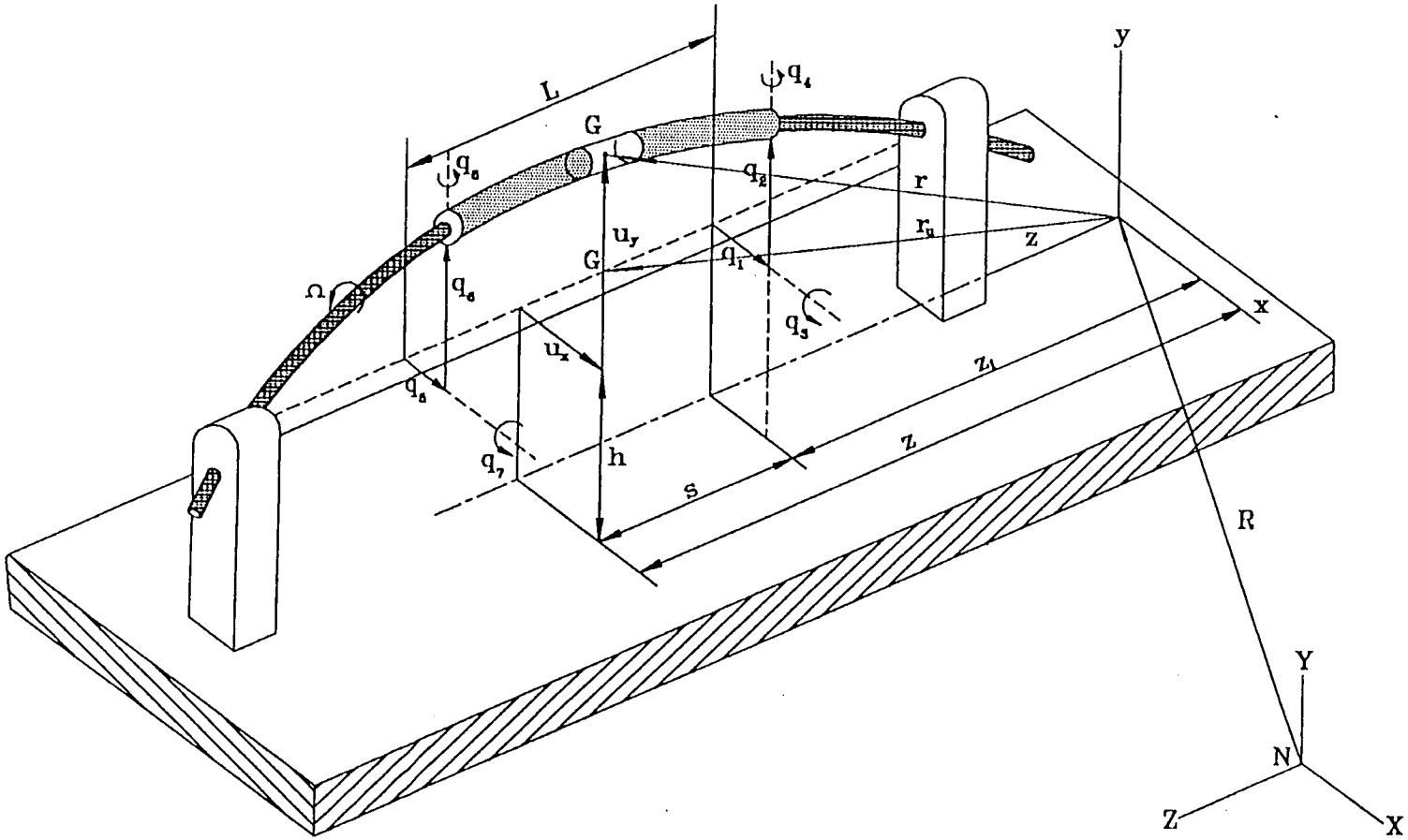

Figure 1. Rotor-bearing system showing nodal coordinates and system of axes.

of the system. Parametric studies to investigate the effects of various system parameters (operating speeds of rotation with forward and reverse directions, shaft flexibility, bearing properties, rigid (pin) supports, and ground motion characteristics) on the dynamic response of the shaft using a Newmark-β time integration scheme are also presented in this chapter. Finally, conclusions regarding the behavior of flexible rotating machines under seismic ground motion are offered.

Chapter II

A Newtonian Approach for Determining the Equations of Motion for a Rotating, Flexible Body

The differential equations for the rotor will be derived by the theory of classical dynamics. The model of a rotor with a constant speed of rotation takes into account bending deformations, rotatory inertia as well as gyroscopic effects. The shaft is assumed rigid in the axial direction and shear deformations of the shaft are neglected.

Let $\mathbf{e}_x$, $\mathbf{e}_y$ and $\mathbf{e}_z$ be mutually perpendicular unit vectors fixed in inertia (Newtonian) reference frame. Let $\mathbf{e}_q$, $\mathbf{e}_r$ and $\mathbf{e}_s$ be a set of mutually perpendicular unit vectors fixed to a differential element B moving in the inertial reference frame N as shown in Figure 2. Assuming small angles, the relationships between unit vectors ($\mathbf{e}_x$, $\mathbf{e}_y$, $\mathbf{e}_z$) and ($\mathbf{e}_q$, $\mathbf{e}_r$, $\mathbf{e}_s$) can be expressed as

$$\begin{bmatrix} e_q \\ e_r \\ e_s \end{bmatrix} = \begin{bmatrix} 1 & 0 & -u' \\ 0 & 1 & -v' \\ u' & v' & 1 \end{bmatrix} \begin{bmatrix} e_x \\ e_y \\ e_z \end{bmatrix} \tag{1}$$

and

$$\begin{bmatrix} e_x \\ e_y \\ e_z \end{bmatrix} = \begin{bmatrix} 1 & 0 & u' \\ 0 & 1 & v' \\ -u' & -v' & 1 \end{bmatrix} \begin{bmatrix} e_q \\ e_r \\ e_s \end{bmatrix} \tag{2}$$

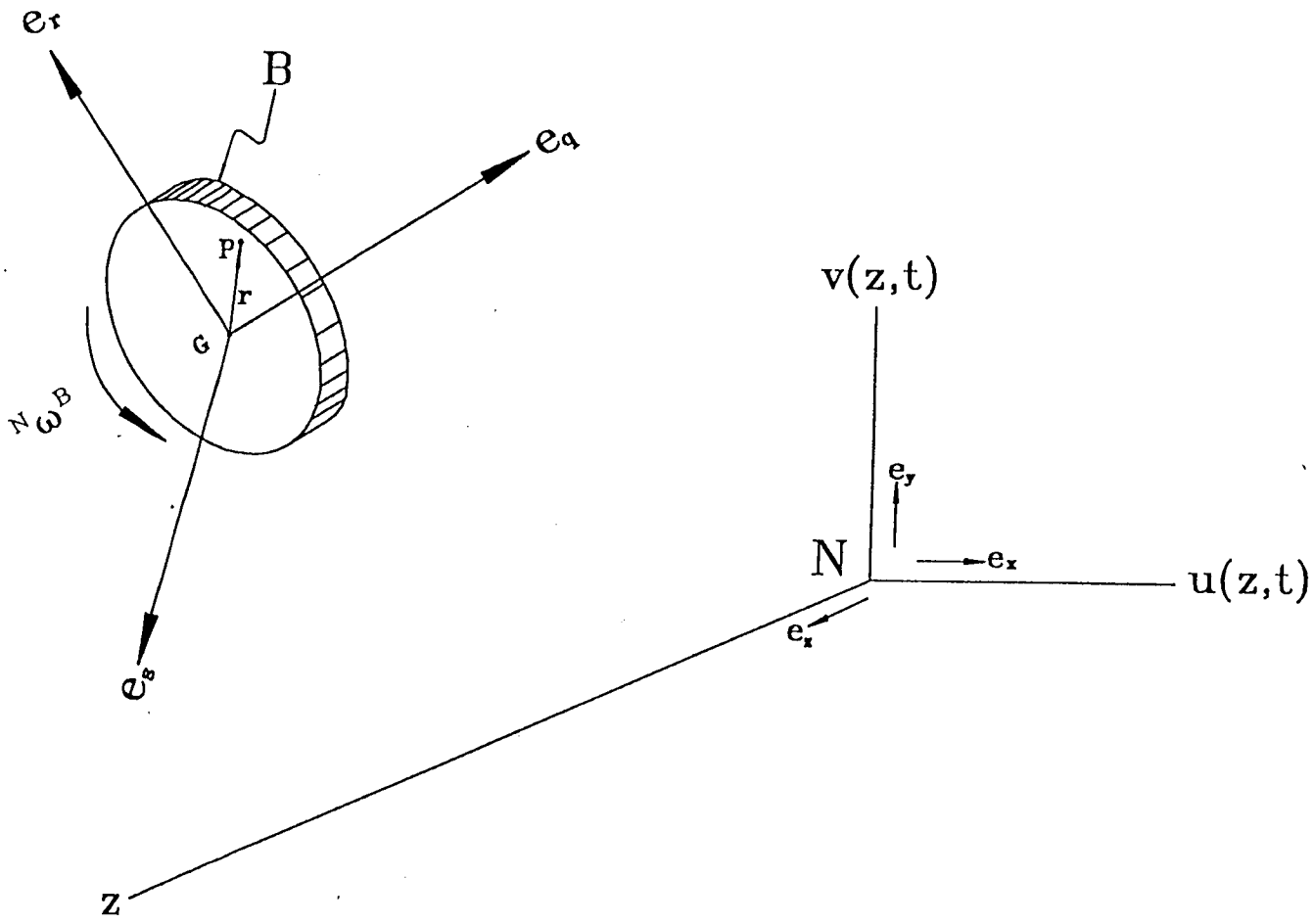

Figure 2. A differential element B moving in the inertia reference frame N.

where u and v are the motions of the differential element of the shaft (shaft deformations) in the x- and y-directions, respectively, and ( )' = d( )/ dz.

Substituting equation (1) into equation (2) and taking derivatives with respect to time, the time derivatives of unit vectors in the relative frame become

$$\dot{e}_q = -\dot{u}'e_z = -\dot{u}'(-u'e_q - v'e_r + e_s)$$

$$\dot{e}_r = -\dot{v}'e_z = -\dot{v}'(-u'e_q - v'e_r + e_s)$$

$$\dot{e}_s = \dot{u}'e_x + \dot{v}'e_y = \dot{u}'(e_q + u'e_s) + \dot{v}'(e_r + v'e_s) \qquad (3)$$

where dot denotes differentiation with respect to time. The angular velocity ${}^N\omega^B$ of a differential element B in the inertial reference frame N (see Figure 2) is defined as [18]

$${}^N\omega^B = e_q\dot{e}_r \cdot e_s + e_r\dot{e}_s \cdot e_q + e_s\dot{e}_q \cdot e_r$$

$$= -\dot{v}'e_q + \dot{u}'e_r + \dot{u}'v'e_s = \Omega_q e_q + \Omega_r e_r \qquad (4)$$

where Ω_q and Ω_r are the angular velocities in the $\mathbf{e}_q$ and $\mathbf{e}_r$ directions, respectively. Since the displacements u and v are small, the term $\dot{u}'v'\mathbf{e}_s$ in the above equation can be neglected in comparison to the other terms. Equating similar terms on the both sides of equation (4) gives $u'=\Omega_r$ and $-v'=\Omega_q$. According to equation (4), the angular acceleration ${}^N\boldsymbol{\alpha}^B$ of differential element B can be obtained by taking the time derivative of the angular velocity which results in

$$^{N}\alpha^{B} = \dot{\Omega}_{q} e_{q} + \dot{\Omega}_{r} e_{r} \tag{5}$$

In order to develop the equations of motion governing the deformations u and v, concepts from the three-dimensional kinetics of rigid bodies will be used [18]. As illustrated in the following development of a "generalized inertia torque", this methodology is an effective means of including gyroscopic and other complex dynamic effects.

Consider a differential element B with symmetric and circular cross section rotating in the inertial reference frame N. Since the shaft is modeled as an Euler-Bernoulli beam, the area of B does not change after deforming, in this case, the particles can not move independently but instead their motions must be such that they maintain fixed distances from each other, preserving the rigidity of B. Let G be the mass center of B, and let P be a typical particle in B as shown in Figure 2. Let $\mathbf{r}$ locate P relative to G. Then the acceleration of P and G in the inertial reference frame N, $^{N}\mathbf{a}^{P}$ and $^{N}\mathbf{a}^{G}$, are related by the expression [18]

$$^{N}\boldsymbol{a}^{P} = {}^{N}\boldsymbol{a}^{G} + {}^{N}\alpha^{B} \times \boldsymbol{r} + {}^{N}\omega^{B} \times ({}^{N}\omega^{B} \times \boldsymbol{r}) \tag{6}$$

where $^{N}\alpha^{B}$ and $^{N}\omega^{B}$ are the angular acceleration and angular velocity of B in the inertial reference frame N. The equivalent inertia torque $\mathbf{M}^{*}$ is defined as

$$\boldsymbol{M}^{*} = -\int_{B} \boldsymbol{r} \times {}^{N}\boldsymbol{a}^{P} \, dm \tag{7}$$

where dm is a differential mass located at P. By substituting equation (6) into equation (7), the inertia torque **M*** becomes

$$\boldsymbol{M}^* = -\int_B \boldsymbol{r}\times[{}^N\boldsymbol{a}^G + {}^N\boldsymbol{\alpha}^B\times\boldsymbol{r} + {}^N\boldsymbol{\omega}^B\times({}^N\boldsymbol{\omega}^B\times\boldsymbol{r})]dm \tag{8}$$

$$= -\int_B \boldsymbol{r}\times{}^N\boldsymbol{a}^G dm - \int_B \boldsymbol{r}\times({}^N\boldsymbol{\alpha}^B\times\boldsymbol{r})dm - \int_B \boldsymbol{r}\times[{}^N\boldsymbol{\omega}^B\times({}^N\boldsymbol{\omega}^B\times\boldsymbol{r})]dm$$

If G is the mass center of B, the sum of the first moments relative to G is zero. That is

$$\int_B \boldsymbol{r}dm = 0 \tag{9}$$

Therefore, the first term in equation (8) is zero. By using the vector identity

$$\boldsymbol{a}\times(\boldsymbol{b}\times\boldsymbol{c}) = (\boldsymbol{a}\cdot\boldsymbol{c})\boldsymbol{b} - (\boldsymbol{a}\cdot\boldsymbol{b})\boldsymbol{c} \tag{10}$$

the last term in equation (8) can be rewritten as

$$-\int_B [\boldsymbol{r}\cdot({}^N\boldsymbol{\omega}^B\times\boldsymbol{r})]{}^N\boldsymbol{\omega}^B dm + \int_B ({}^N\boldsymbol{\omega}^B\cdot\boldsymbol{r}){}^N\boldsymbol{\omega}^B\times\boldsymbol{r}dm \tag{11}$$

Note that the first term in equation (11) is zero since $\mathbf{r}$ is perpendicular to ${}^N\boldsymbol{\omega}^B\times\mathbf{r}$. The second term in equation (11) can be expressed as

$$\int_B [(r\cdot {}^N\omega^B){}^N\omega^B \times r - ({}^N\omega^B \cdot {}^N\omega^B \times r)r]dm$$

$$= -\int_B {}^N\omega^B \times [r \times ({}^N\omega^B \times r)]dm$$

$$= -{}^N\omega^B \times \int_B [r \times ({}^N\omega^B \times r)]dm \qquad (12)$$

Therefore, the inertia torque **M*** in equation (8) can be rewritten as

$$M^* = -\int_B r \times ({}^N\alpha^B \times r)dm - {}^N\omega^B \times \int_B r \times ({}^N\omega^B \times r)dm \qquad (13)$$

Suppose that ${}^N\alpha^B$ and ${}^N\omega^B$ are expressed as

$${}^N\alpha^B = |{}^N\alpha^B| e_i = \alpha e_i \; ; \; {}^N\omega^B = |{}^N\omega^B| = \omega e_i \quad (i=q,r,s) \qquad (14)$$

where α and ω are defined as the magnitude of ${}^N\alpha^B$ and ${}^N\omega^B$, respectively, and $\mathbf{e}_i$ are the unit vectors shown in Figure 2. Then using equation (14), the first term of equation (13) is

$$\alpha \int_B r \times (e_i \times r)dm \qquad (15)$$

while the second term of equation (13) is

$$\omega^N\omega^B \times \int_B r \times (e_i \times r)dm \qquad (16)$$

Thus the expression for the inertia torque in equation (13) is

$$\boldsymbol{M}^* = -\alpha \int_B \boldsymbol{r}\times(\boldsymbol{e}_i\times\boldsymbol{r})dm - \omega^N\omega^B\times\int_B \boldsymbol{r}\times(\boldsymbol{e}_i\times\boldsymbol{r})dm \tag{17}$$

The inertia matrix **I** is defined as

$$\boldsymbol{I} = \int \boldsymbol{r}\times(\boldsymbol{e}_i\times\boldsymbol{r})dm \tag{18}$$

The inertia matrix $\mathbf{I}^{B/G}$ of the differential element B relative to the mass center G is, for mutually perpendicular unit vectors $\mathbf{e}_q$, $\mathbf{e}_r$ and $\mathbf{e}_s$ shown in Figure 2

$$\boldsymbol{I}^{B/G} = \begin{bmatrix} I_{qq} & 0 & 0 \\ 0 & I_{rr} & 0 \\ 0 & 0 & I_{ss} \end{bmatrix} = \begin{bmatrix} I & 0 & 0 \\ 0 & I & 0 \\ 0 & 0 & J \end{bmatrix} \tag{19}$$

In the above, I is mass moment of inertia relative to either $\mathbf{e}_q$ or $\mathbf{e}_r$, while J is the polar moment of inertia for the circular cross section. Note that I=1/2J. Using the definitions, the inertia torque in equation (17) can be rewritten as

$$\boldsymbol{M}^* = -\boldsymbol{I}^{B/G}\cdot{}^N\alpha^B - {}^N\omega^B\times(\boldsymbol{I}^{B/G}\cdot{}^N\omega^B) \tag{20}$$

The components of ${}^N\omega^B$ parallel and perpendicular to ${}^N\omega^B$ are expressed as

$$\omega^B = (e_s \cdot {}^N\omega^B)e_s + (e_s \times {}^N\omega^B) \times e_s \tag{21}$$

Combining equation (21) with equation (19), we have

$$I^{B/G,N}\omega^B = Je_s \cdot {}^N\omega^B e_s + I(e_s \times {}^N\omega^B) \times e_s \tag{22}$$

Taking the cross product between ${}^N\omega^B$ and both sides of equation (22) results in

$${}^N\omega^B \times (I^{B/G,N}\omega^B) = {}^N\omega^B \times [J\Omega_s e_s + I(e_s \times {}^N\omega^B) \times e_s]$$

$$= {}^N\omega^B \times J\Omega_s e_s \tag{23}$$

Substituting equation (23) into equation (20) and using equations (4) and (5), the inertia torque M* becomes

$$M^* = -(I\dot{\Omega}_q - J\Omega_s\Omega_r)e_q - (I\dot{\Omega}_r + J\Omega_s\Omega_q)e_r \tag{24}$$

In general, the mass moment and polar mass moment of an element of the shaft with length dz can be expressed as

$$I = \rho A k^2 dz \; ; \; J = 2\rho A k^2 dz \tag{25}$$

where ρ and A are the mass density and cross sectional area of the shaft, respectively. The radius of gyration of the cross section is k^2(=I/A). In classical dynamics, the equivalent equation of the generalized active torque M and inertia torque M* is expressed as

$$\boldsymbol{M} + \boldsymbol{M}^* = 0 \tag{26}$$

The above equivalent equation is simply an expression of d'Alembert's principle. Referring to Figure 3, the moment acting on the differential element is

$$\boldsymbol{M} = [M_x(z+dz) - M_x(z) - V_y(z)dz]\boldsymbol{e}_q + [M_y(z+dz) - M_y(z) + V_x(z)dz]\boldsymbol{e}_r \tag{27}$$

The shaft is assumed to be a Bernoulli-Euler beam when the slopes of the deflection curve are very small and neglect the shear deformations, M_x=-EIv" and M_y=EIu". Combining these expressions with equations (24) - (27) and the kinematic relations (Ω_r=u', Ω_q=-v'), resulting in

$$\frac{\partial^2}{\partial z^2}[EI\frac{\partial^2 u}{\partial z^2}] - \frac{\partial^2}{\partial z^2}[mk^2(\frac{\partial^2 u}{\partial t^2} - 2\Omega_s\frac{\partial v}{\partial t})] + m\frac{\partial^2 u}{\partial t^2} = 0 \tag{28}$$

$$\frac{\partial^2}{\partial z^2}[EI\frac{\partial^2 v}{\partial z^2}] - \frac{\partial^2}{\partial z^2}[mk^2(\frac{\partial^2 v}{\partial t^2} + 2\Omega_s\frac{\partial u}{\partial t})] + m\frac{\partial^2 v}{\partial t^2} = 0 \tag{29}$$

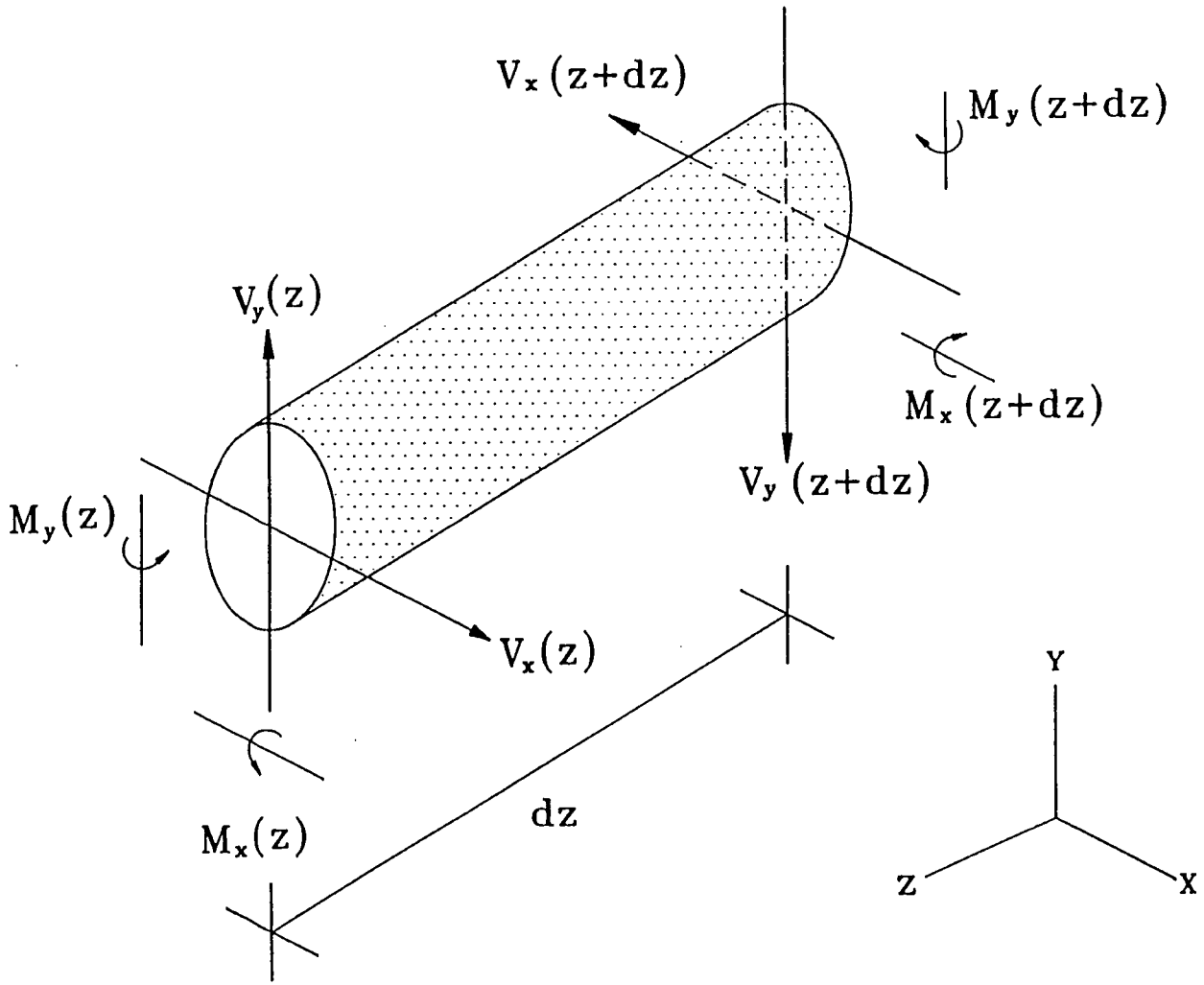

Figure 3. Free-Body diagram of the differential element of the shaft.

where $m(=\rho A)$ is mass per unit length.

The governing equations of motion given above for the free-vibration of a shaft rotating with constant angular velocity were derived by Newtonian mechanics. These coupled partial differential equations can, in principle, be used to determine the response of a rotating, flexible shaft with various properties along the length of the shaft and appropriate boundary conditions at the supports. The applications of these coupled partial differential equations to determine the vibration frequency and the critical speed of the rotating system will be discussed in chapter IV. In the subsequent chapter, energy and finite element methods will be used to obtain the equations of motion.

Chapter III

Finite Element Equations for the Rotating, Flexible Shaft by an Energy Approach

III. 1 Energy methods for the differential equations

The finite element equations of motion for the rotating, flexible shaft will be derived using energy methods. The shaft is modeled as a Bernoulli-Euler beam with circular cross section. The properties of the shaft may vary along the length. It is assumed that the shaft is rigid in the axial direction and shear deformations of the shaft are neglected. The motion is described by two reference frames as shown in Figure 1. The Newtonian reference frame, (X,Y,Z) system, maintains a fixed orientation in space while the local reference frame, (x,y,z) system, is attached to the base of the machine. Translational motion of the base can be described by a vector R from the origin of the Newtonian frame to a typical point on the base. The components of R are X_b,Y_b and Z_b. The shaft is spinning with a constant angular velocity Ω about the z-axis. The location of a typical point G on the shaft is given with respect to the local coordinate axes (x,y,z) by the contributions vector r_u=(0, h, z) where h is the height of the shaft from base and z is location point G with respect to the local frame. In the deformed shaft point G is located at r=(u_x, u_y+h, z) where u_x and u_y are the contributions to the displacement vector due to the flexibility of the shaft.

The kinetic energy of a typical differential element separates into two independent parts: (i) the translational kinetic energy, dT_{trans} and (ii) the rotational kinetic energy, dT_{rot};

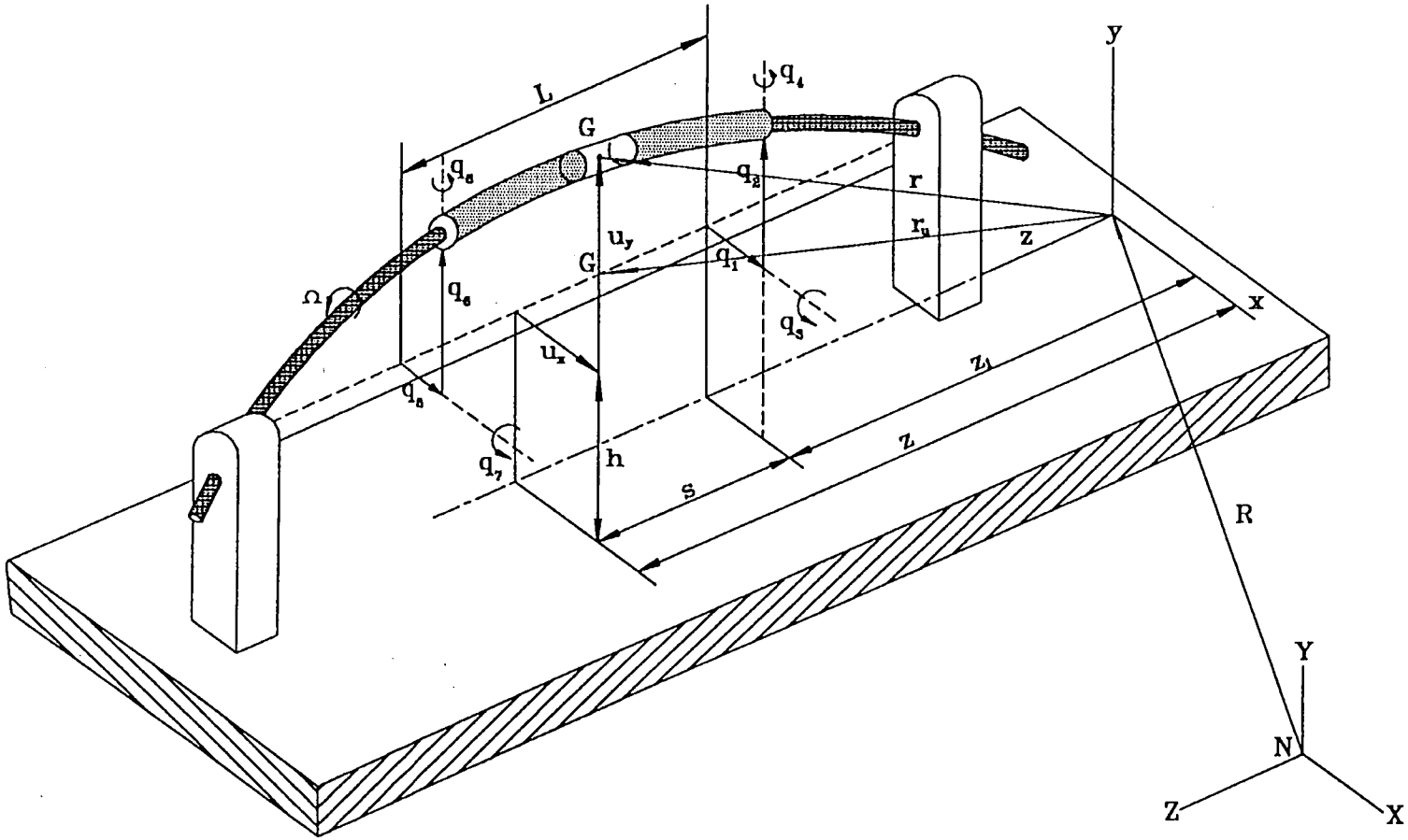

Figure 1. Rotor-bearing system showing nodal coordinates and system of axes.

i.e.

$$dT = dT_{trans} + dT_{rot} \tag{30}$$

where

$$dT_{trans} = \frac{1}{2} v_g^T v_g dm \tag{31}$$

and

$$dT_{rot} = \frac{1}{2} \sum_{i,j=1}^{3} I_{ij} \omega_i \omega_j \tag{32}$$

The angular velocities and moments of inertia of the differential element are ω_i and I_{ij}, respectively. The velocity v_g of the point G on the deformed shaft with respect to the Newtonian frame is defined as the sum of the velocity of the base v_b relative to the Newtonian frame and the velocity of the differential element point G, $\dot{r}$, relative to the local reference frame, i.e.

$$v_g = v_b + \dot{r} \tag{33}$$

and

$$v_b = \begin{bmatrix} \dot{X}_b \\ \dot{Y}_b \\ \dot{Z}_b \end{bmatrix} \tag{34}$$

Referring to equation (32), note that if a shaft rotates around a principal axis, both angular velocity and the angular momentum are directed along this axis; then, the inertia tensor I_{ij} consists solely of diagonal elements. Such axes are termed principal axes of inertia. A considerable simplification in the expressions for the rotational kinetic energy of the differential element dT_{rot} can be written for principal axes of inertia, i.e.

$$dT_{rot} = \frac{1}{2}\sum_{i=1}^{3} I_i \omega_i^2 \tag{35}$$

where I_i are the principal moments of inertia of the differential element.

Substituting equation (33) into equation (31), the translational kinetic energy of the differential element then can be written as

$$dT_{trans} = \frac{1}{2}\rho A(v_b{}^T v_b + \dot{r}^T \dot{r})dz \tag{36}$$

where ρ and A are the mass density and the cross-sectional area of the differential element, respectively.

In equation (35), the angular velocity ω_i can be written in terms of the Eulerian angles [20], θ_x (about x-axis), θ_y (about y-axis) and Ωt (about z-axis) where θ_x and θ_y are the rotations of the differential element due to bending and t is the time, as

$$\begin{bmatrix}\omega_1\\ \omega_2\\ \omega_3\end{bmatrix} = \begin{bmatrix}\cos\theta_y\cos\Omega t & \sin\Omega t & 0\\ -\cos\theta_y\sin\Omega t & \cos\Omega t & 0\\ \sin\theta_y & 0 & 1\end{bmatrix}\begin{bmatrix}\dot{\theta}_x\\ \dot{\theta}_y\\ \Omega\end{bmatrix} \tag{37}$$

Assuming small Eulerian angles, the angular velocities in equation (37) become

$$\begin{aligned}\omega_1 &= \dot{\theta}_x + \Omega t\dot{\theta}_y\\ \omega_2 &= -\dot{\theta}_x\Omega t + \dot{\theta}_y\\ \omega_3 &= \theta_y\dot{\theta}_x + \Omega\end{aligned} \tag{38}$$

The rotational kinetic energy of differential element dT_{rot} in equation (35) can be expressed as

$$dT_{rot} = \frac{1}{2}\sum_{i=1}^{3} I_i\omega_i^2 = \frac{1}{2}(I_{\bar{x}}\omega_1^2 + I_{\bar{y}}\omega_2^2 + I_{\bar{z}}\omega_3^2) \tag{39}$$

$$= \frac{1}{2}[I_{\bar{x}}\dot{\theta}_x^2 + I_{\bar{x}}\dot{\theta}_y^2 + 2I_{\bar{z}}\Omega\theta_y\dot{\theta}_x + I_{\bar{z}}\Omega^2 + I_{\bar{x}}\Omega^2t^2\dot{\theta}_y^2 + I_{\bar{y}}\Omega^2t^2\dot{\theta}_x^2 + I_{\bar{z}}\theta_y^2\dot{\theta}_x^2]$$

where $I_{\bar{x}}$, $I_{\bar{y}}$ and $I_{\bar{z}}$ ($I_{\bar{x}} = I_{\bar{y}} = 1/2\ I_{\bar{z}}$) are moments of inertia of the cross sectional area about

x-, y- and z-direction with respect to centroidal axis of shaft, respectively. Since the Eulerian angles θ_x, θ_y, Ωt and their first derivative with respect to time are assumed to be small, i.e. of order ϵ where $\epsilon << 1$; then the last three terms can be neglected. Equation (39) can be written in matrix form as

$$dT_{rot} = \frac{1}{2}\rho(I_{\bar{x}}\dot{\varphi}^T\dot{\varphi} + 2\Omega I_{\bar{z}}\dot{\varphi}^T e_1 e_2^T \varphi + \Omega^2 I_{\bar{z}})dz \tag{40}$$

The vectors introduced in the above equation are

$$\varphi = \begin{bmatrix}\theta_x\\ \theta_y\\ 0\end{bmatrix};\ e_1 = \begin{bmatrix}1\\ 0\\ 0\end{bmatrix};\ e_2 = \begin{bmatrix}0\\ 1\\ 0\end{bmatrix} \tag{41}$$

Let

$$u = \begin{bmatrix}u_x\\ u_y\\ 0\end{bmatrix} \tag{42}$$

According to Bernoulli-Euler theory (i.e. in the absence of shear deformations), $\theta_x = -u_y'$ and $\theta_y = u_x'$, the potential energy dV can be expressed in terms of the internal bending strain energy of the differential element, i.e.

$$dV = \frac{1}{2}(EI_x \boldsymbol{u}''^T \boldsymbol{u}'')dz \tag{43}$$

where E is the Young's modulus.

III. 2 Finite element equations (shear deformations neglected)

Consider a typical finite element of length L^e. The displacements and rotations for a typical element are u^e and φ^e. These quantities can be expressed in terms of the nodal displacements through interpolation functions as

$$\boldsymbol{u}^e = [u_x{}^e(s), u_y{}^e(s), 0]^T = \boldsymbol{N}\boldsymbol{q}^e$$

$$\boldsymbol{\varphi}^e = [\theta_x{}^e(s), \theta_y{}^e(s), 0]^T = \boldsymbol{N}'\boldsymbol{q}^e \tag{44}$$

where **N** is the matrix of interpolation functions; **N'** is the first derivative of **N**; q^e are the nodal quantities and s is a local coordinate measured along the length of a finite element. The vector r appearing in equation (36) can also be expressed in terms of nodal displacements as

$$\boldsymbol{r} = \boldsymbol{u}^e + \boldsymbol{e} \tag{45}$$

$$\boldsymbol{e} = \begin{bmatrix} 0 \\ h \\ z_1 + s \end{bmatrix} \tag{46}$$

where the location of the left end of the finite element with respect to the xyz coordinate system is z_1.

The Lagrangian of a particular finite element (L^e) can be obtained by integrating the difference between the kinetic and potential energies from equations (36), (40) and (43) over the length of the finite element. The nodal degrees of freedom of the element q_i^e are the generalized coordinates of Lagrange's method. Applying Lagrange's equations directly,

$$\frac{\partial L^e}{\partial q_i^e} - \frac{d}{dt}\frac{\partial L^e}{\partial \dot{q}_i^e} = 0; \ (i=1,2,....,n) \tag{47}$$

where

$$L^e = \int_0^l (dT^e - dV^e) \tag{48}$$

one obtains the element equations of motion, i.e.

$$\boldsymbol{M}^e\ddot{\boldsymbol{q}}^e + \boldsymbol{C}^e\dot{\boldsymbol{q}}^e + \boldsymbol{K}^e\boldsymbol{q}^e = \boldsymbol{f}^e(t) \tag{49}$$

where the element mass, damping, stiffness and applied force matrices are defined as

$$\boldsymbol{M}^e = \int_0^l \rho A \boldsymbol{N}^T \boldsymbol{N} ds + \int_0^l \rho I_x \boldsymbol{N}'^T \boldsymbol{N}' ds \tag{50}$$

$$C^e = \Omega \int_0^l I_p N'^T (e_1 e_2^T - e_2 e_1^T) N' ds \tag{51}$$

$$K^e = \int_0^l E I_x N''^T N'' ds \tag{52}$$

$$f^e(t) = -\int_0^l [\rho A N^T ds] \dot{v}_b \tag{53}$$

where ρ is the mass density of the shaft and $\dot{v}_b$ is the vector of translational base accelerations.

Referring to equation (44), in order to satisfy continuity requirements, the interpolation functions must be assumed as continuous in displacement and slope on the element boundaries, i.e. C' continuity. Thus appropriate nodal quantities are displacements and rotations at each end of the element (see Figure 4). The cubic beam (Hermite) polynomials satisfy C' continuity and are an appropriate choice for the interpolation function N. The matrix of the cubic interpolation functions **N** is

$$N = \begin{bmatrix} n_1 & 0 & n_2 & 0 & n_3 & 0 & n_4 & 0 \\ 0 & n_1 & 0 & n_2 & 0 & n_3 & 0 & n_4 \\ 0 & 0 & 0 & 0 & 0 & 0 & 0 & 0 \end{bmatrix} \tag{54}$$

where

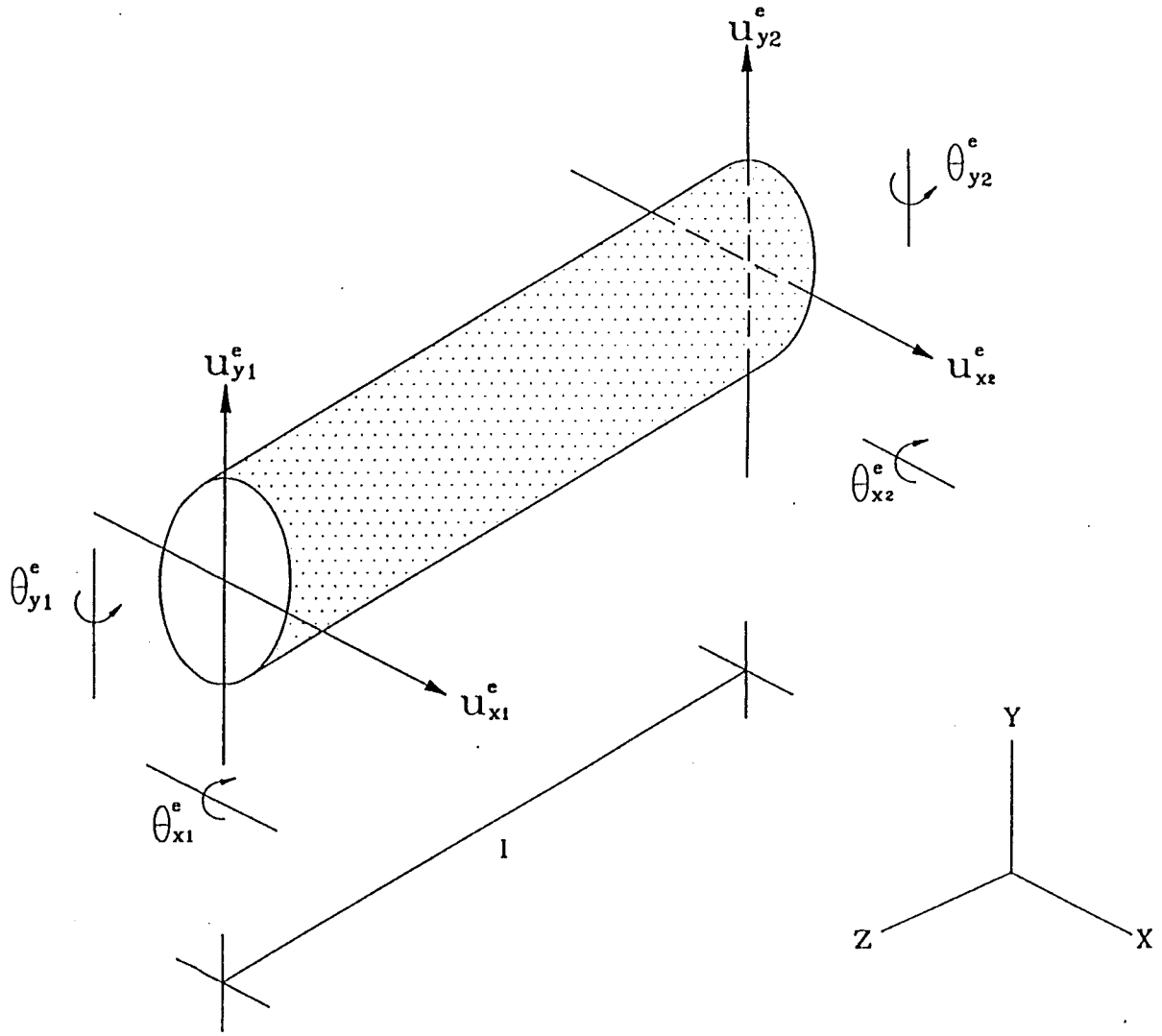

Figure 4. Nodal displacements and rotations of a typical element of the shaft.

$$n_1 = 1 - \frac{3}{l^2}s^2 + \frac{2}{l^3}s^3$$

$$n_2 = s - \frac{2}{l}s^2 + \frac{1}{l^2}s^3$$

$$n_3 = \frac{3}{l^2}s^2 - \frac{2}{l^3}s^3$$

$$n_4 = \frac{1}{l^2}s^3 - \frac{1}{l}s^2 \qquad (55)$$

Because each finite element has two nodes (at the left and right ends of the element), there are four degrees of freedom at each node; two translational degrees of freedom (u_x^e, u_y^e) and two rotational degrees of freedom (θ_x^e, θ_y^e) in the x- and y-directions; therefore, q^e in equation (49) is an 8×1 vector of nodal displacements and rotations given by

$$\boldsymbol{q}^e = \boldsymbol{q}_i^{eT} = [u_{x1}^e, u_{y1}^e, \theta_{x1}^e, \theta_{y1}^e, u_{x2}^e, u_{y2}^e, \theta_{x2}^e, \theta_{y2}^e]^T \qquad (56)$$

$$(i=1,2,.....,8)$$

where the second subscripts 1 and 2 indicate the nodal displacements of the left and right ends of the element, respectively.

The flexible shaft may be modelled as Timoshenko beam (considering the effects of shear deformations), carry one or more disks and is supported by journal-fluid bearings at the ends (see Figure 5). These issues are discussed in the following sections.

III. 3 Finite element equations (including shear deformations)

When the shaft of a rotating machine is short and stocky, the effect of transverse shear on the response of the shaft can not be neglected. The effects of shear deformations should be included in the analysis of the shaft.

When the effects of shear deformations are considered in the analysis and the same interpolation functions are used to approximate the transverse deflection and the rotation, the resulting stiffness matrix is often too stiff. This is due to the inconsistency of interpolation of the variables, and the phenomenon is known as "shear locking". In order to overcome this problem, the methods of consistent interpolation element (CIE) and reduced integration element (RIE) have been developed by Reddy [21]. In practical applications, the stiffness matrix of the shaft obtained by the methods of CIE or RIE are not so straightforward. An apparently simple formulation to modify the stiffness matrix of equation (52) by using the method of superposition [17] is derived below.

In what follows, only the x-direction will be considered. The treatment is identical for the y-direction. The transverse displacements of the shaft can be expressed by superposing bending and shear displacements, i.e.

$$u_x^{\,e} = u_x^{\,eb} + u_x^{\,es} \tag{57}$$

where $u_x^{\,e}$ is the total element transverse displacement; $u_x^{\,eb}$ and $u_x^{\,es}$ are the element transverse displacements due to bending and shear deformations, respectively. The element transverse displacements $u_x^{\,eb}$ and $u_x^{\,es}$ defined in terms of interpolation functions

and nodal values are

$$u_x^{eb} = n_1 u_{x1}^{eb} + n_2 \theta_{x1}^{eb} + n_3 u_{x2}^{eb} + n_4 \theta_{x2}^{eb} \tag{58}$$

$$u_x^{es} = n_5 u_{x1}^{es} + n_6 u_{x2}^{es} \tag{59}$$

where n_1, n_2, n_3 and n_4 are cubic interpolation functions defined in equation (55); n_5, n_6 are linear interpolation functions (n_5=1-s/l, n_6=s/l). There is no rotation of the cross section due to shear deformations; therefore, a linear interpolation function can be used to approximate the shear deformations.

Similarly, the nodal displacements and rotations can be expressed in two parts: (i) the nodal displacements and rotations due to bending q_b^e and (ii) the nodal displacements due to shear q_s^e, i.e.

$$q_b^e = \begin{bmatrix} u_{x1}^{eb} \\ \theta_{x1}^{eb} \\ u_{x2}^{eb} \\ \theta_{x2}^{eb} \end{bmatrix} \tag{60}$$

and

$$q_s^e = \begin{bmatrix} u_{x1}^{es} \\ u_{x2}^{es} \end{bmatrix} \tag{61}$$

The element strains can be expressed as

$$\varepsilon^{eb}(z)=\boldsymbol{B}^{eb}\boldsymbol{q}_b^{\,e};\ \varepsilon^{es}(z)=\boldsymbol{B}^{es}\boldsymbol{q}_s^{\,e} \tag{62}$$

where $\varepsilon^{eb}(z)$ and $\varepsilon^{es}(z)$ are element bending and shear strains, respectively; B^{eb} and B^{es} are defined as

$$\boldsymbol{B}^{eb} = \left[\frac{12s-6l}{l^3} \quad \frac{6sl-4l^2}{l^3} \quad \frac{-12s+6l}{l^3} \quad \frac{6sl-2l^2}{l^3}\right] \tag{63}$$

and

$$\boldsymbol{B}^{es} = \left[-\frac{1}{l} \quad \frac{1}{l}\right] \tag{64}$$

The element stress can be expressed as

$$\sigma^{eb}= D^{eb}\varepsilon^{eb};\ \sigma^{es}= D^{es}\varepsilon^{es} \tag{65}$$

where D^{eb}=EI and D^{es}=kGA.

Consider an element with nodal forces $P^e=[Q_{x1}^{\,e}, M_{x1}^{\,e}, Q_{x2}^{\,e}, M_{x2}^{\,e}]^T$. Using the principle of virtual displacement, the external virtual work δW_E of the applied nodal forces

is given by

$$\delta W_E = Q_{x1}{}^e(\delta u_{x1}{}^{eb} + \delta u_{x1}{}^{es}) + Q_{x2}{}^e(\delta u_{x2}{}^{eb} + \delta u_{x2}{}^{es}) + M_{x1}{}^e \delta\theta_{x1}{}^{eb} + M_{x2}{}^e \delta\theta_{x2}{}^{eb} \tag{66}$$

The internal virtual work δW_I is the sum of two parts, one due to bending and one due to shear, i.e.

$$\delta W_I = \int_0^l \delta \varepsilon^{eb} \sigma^{eb} dx + \int_0^l \delta \varepsilon^{es} \sigma^{es} dx \tag{67}$$

Substituting equations (62) and (65) into equation (67) and equating external and internal work, the equilibrium equation can be expressed as

$$\delta \boldsymbol{q}_b{}^{eT} \int_0^l \boldsymbol{B}^{ebT} D^{eb} \boldsymbol{B}^{eb} dx \boldsymbol{q}_b{}^e + \delta \boldsymbol{q}_s{}^{eT} \int_0^l \boldsymbol{B}^{esT} D^{eb} \boldsymbol{B}^{eb} dx \boldsymbol{q}_s{}^e$$

$$= \delta \boldsymbol{q}_b{}^{eT} \boldsymbol{P}^e + \delta \boldsymbol{q}_s{}^{eT} \begin{bmatrix} Q_{x1}{}^e \\ Q_{x2}{}^e \end{bmatrix} \tag{68}$$

Since the virtual displacement δ is arbitrary, the above equation yields

$$\int_0^l \boldsymbol{B}^{ebT} D^{eb} \boldsymbol{B}^{eb} dx \boldsymbol{q}_b{}^e = \boldsymbol{P}^e \tag{69}$$

$$\int_0^l \boldsymbol{B}^{es^T} D^{es} \boldsymbol{B}^{es} dx \boldsymbol{q}_s^{\,e} = \begin{bmatrix} Q_{x1}^{\,e} \\ Q_{x2}^{\,e} \end{bmatrix} \tag{70}$$

Equations (69) and (70) can be written as

$$\boldsymbol{K}_b^{\,e} \boldsymbol{q}_b^{\,e} = \boldsymbol{P}^e \; ; \; \boldsymbol{K}_s^{\,e} \boldsymbol{q}_s^{\,e} = \begin{bmatrix} Q_{x1}^{\,e} \\ Q_{x2}^{\,e} \end{bmatrix} \tag{71}$$

where

$$\boldsymbol{K}_b^{\,e} = \begin{bmatrix} \frac{12EI}{l^3} & -\frac{6EI}{l^2} & -\frac{12EI}{l^3} & -\frac{6EI}{l^2} \\ -\frac{6EI}{l^2} & \frac{4EI}{l} & \frac{6EI}{l^2} & \frac{2EI}{l} \\ -\frac{12EI}{l^3} & \frac{6EI}{l^2} & \frac{12EI}{l^3} & \frac{6EI}{l^2} \\ -\frac{6EI}{l^2} & \frac{2EI}{l} & \frac{6EI}{l^2} & \frac{4EI}{l} \end{bmatrix} \tag{72}$$

$$\boldsymbol{K}_s^{\,e} = kGA \begin{bmatrix} \frac{1}{l} & -\frac{1}{l} \\ -\frac{1}{l} & \frac{1}{l} \end{bmatrix} \tag{73}$$

In the above G and k are the shear modulus and shear correction factor. The shear correction factor for a circular cross-section is

$$k = \frac{6(1+\nu)}{7+6\nu} \tag{74}$$

where ν is Poisson ratio. The shear forces at the nodes due to external applied forces can be obtained from equation (71)

$$\frac{EI}{l^3}\begin{bmatrix}12 & -6l\end{bmatrix}\begin{bmatrix}u_{x1}^{eb}-u_{x2}^{eb}\\ \theta_{x1}^{eb}+\theta_{x2}^{eb}\end{bmatrix} = Q_{x1}^{e} = -Q_{x2}^{e} \tag{75}$$

and

$$\frac{kGA}{l}[u_{x1}^{es}-u_{x2}^{es}] = Q_{x1}^{e} = -Q_{x2}^{e} \tag{76}$$

Equating (75) and (76),

$$\frac{EI}{l^3}\begin{bmatrix}12 & -6l\end{bmatrix}\begin{bmatrix}u_{x1}^{eb}-u_{x2}^{eb}\\ \theta_{x1}^{eb}+\theta_{x2}^{eb}\end{bmatrix} = \frac{kGA}{l}(u_{x1}^{es}-u_{x2}^{es}) \tag{77}$$

Expanding equation (77) results in

$$u_{x1}^{es}-u_{x2}^{es} = b[(u_{x1}^{eb}-u_{x2}^{eb})-\frac{l}{2}(\theta_{x1}^{eb}+\theta_{x2}^{eb})] \tag{78}$$

where $b=12EI/(kGAl^2)$ is the effect factor of shear deformation. When $b<<1$, the shear deformations can be ignored relative to the bending deformations. From equation (57), the relationships of nodal displacement have

$$u_{x1}^{es} = u_{x1}^{e} - u_{x1}^{eb};\ u_{x2}^{es} = u_{x2}^{e} - u_{x2}^{eb} \tag{79}$$

Combining equations (78) and (79)

$$u_{x1}^{eb} - u_{x2}^{eb} = \frac{1}{(1+b)}(u_{x1}^{e} - u_{x2}^{e}) + \frac{bl}{2(1+b)}(\theta_{x1}^{eb} + \theta_{x2}^{eb}) \tag{80}$$

Elements of the modified stiffness matrix for a shaft element with shear deformations in the x-direction can be obtained by changing u_{x1}^{eb} and u_{x2}^{eb} of $\mathbf{q}_b^e$ in equation (71) with the total transverse displacements, u_{x1}^{e} and u_{x2}^{e} in equation (80). The stiffness matrix K_x^e including shear deformations in the x-direction is

$$\boldsymbol{K}_x^e = \begin{bmatrix} \frac{12EI}{(1+b)l^3} & -\frac{6EI}{(1+b)l^2} & -\frac{12EI}{(1+b)l^3} & -\frac{6EI}{(1+b)l^2} \\ -\frac{6EI}{(1+b)l^2} & \frac{(4+b)EI}{(1+b)l} & \frac{6EI}{(1+b)l^2} & \frac{(2-b)EI}{(1+b)l} \\ -\frac{12EI}{(1+b)l^3} & \frac{6EI}{(1+b)l^2} & \frac{12EI}{(1+b)l^3} & \frac{6EI}{(1+b)l^2} \\ -\frac{6EI}{(1+b)l^2} & \frac{(2-b)EI}{(1+b)l} & \frac{6EI}{(1+b)l^2} & \frac{(4+b)EI}{(1+b)l} \end{bmatrix} \tag{81}$$

For the stiffness matrix K_y^e including shear deformations in the y-direction, the same procedures apply as for the matrix K_x^e . The complete stiffness matrix K^e including shear deformation in x- and y-directions can be obtained by appropriately adding matrices K_x^e and K_y^e.

III. 4 Rigid disks

A rotating machine may be carrying several rigid disks along the shaft. To consider the effects of these rigid disks on the response of the flexible shaft, they can be modelled as thin rigid disks with concentrated mass applied to the finite element nodes. Similarly, the equations of motion for the rigid disk can be derived using energy and Lagrange's methods.

The displacements and rotations at an arbitrary point in a typical element of the shaft are given in equations (44) and (54). Without loss of generality, assume a rigid disk is attached to the left end (s=0 location) of a typical element. Since the disk is attached to only one end, the quantities of equation (56) are

$$\boldsymbol{u}_d^e = \boldsymbol{u}^e(s=0) = \boldsymbol{A}\boldsymbol{q}_d^e \tag{82}$$

where

$$\boldsymbol{q}_d^e = [u_x, u_y, \theta_x, \theta_y]^T$$

$$A = \begin{bmatrix} 1 & 0 & 0 & 0 \\ 0 & 1 & 0 & 0 \\ 0 & 0 & 0 & 0 \end{bmatrix} \tag{83}$$

Note that

$$u_d^{e\prime} = u^{e\prime}(s=0) = A' q_d^e \tag{84}$$

where

$$A' = \begin{bmatrix} 0 & 0 & 1 & 0 \\ 0 & 0 & 0 & 1 \\ 0 & 0 & 0 & 0 \end{bmatrix} \tag{85}$$

Since we are only considering the effect of attaching a rigid disk to the element, the internal bending strain energy is zero. Therefore, the potential energy term dV^e in equation (48) will vanish. The equations of motion can be obtained by using the Lagrange equations directly in a manner similar to the previous section, resulting in

$$M_d^e \ddot{q}_d^e + C_d^e \dot{q}_d^e + K_d^e q_d^e = f^e{}_d(t) \tag{86}$$

The mass, damping, stiffness and applied force matrices are

$$\boldsymbol{M}_d{}^e = m_d \boldsymbol{A}^T \boldsymbol{A} + I_t \boldsymbol{A}'^T \boldsymbol{A}'$$

$$\boldsymbol{C}_d{}^e = \Omega I_0 \boldsymbol{A}'^T [\boldsymbol{e}_1 \boldsymbol{e}_2{}^T - \boldsymbol{e}_2 \boldsymbol{e}_1{}^T] \boldsymbol{A}'$$

$$\boldsymbol{K}_d{}^e = \boldsymbol{0}$$

$$\boldsymbol{f}^e{}_d(t) = -m_d \boldsymbol{A}^T \dot{\boldsymbol{v}}_b \qquad (87)$$

where m_d = mass of disk , I_t = transverse mass moment of inertia, I_0 = polar mass moment of inertia.

III. 5 Journal-fluid-bearing system

To obtain the equations of motion of the complete shaft, the stiffness and damping characteristics of the journal-fluid-bearing system must be considered. The bearing system is often the major source to provide significant stiffness as well as damping for the rotating machine. The bearing affects the critical speeds and the stability of the rotor. Fluid-film bearings are generally modeled by two linear orthogonal elastic and damping forces which depend on the displacements and velocities at the bearing location, respectively [22]. The fluid-film reaction force is a function of the speed of rotation, journal length, journal diameter, radial clearance, lubricant viscosity and the weight of the bearing. The stiffness and damping characteristics of the bearing with

L/D = 1 are given by Earles et al. [23]

$$C_{ij}^{\,b} = \frac{W\bar{c}_{ij}}{h} \quad (i,j=1,2) \tag{88}$$

$$K_{ij}^{\,b} = \frac{W\bar{k}_{ij}}{h} \quad (i,j=1,2) \tag{89}$$

where W, h, D and L are the weight on bearing, radial clearance, journal diameter and bearing length respectively; k_{ij} and c_{ij} are

$$\bar{k}_{11} = 1.512 - 3.218s + 0.889s^2$$

$$\bar{k}_{12} = -0.73 + 18.217s + 1.67s^2$$

$$\bar{k}_{21} = -2.677 - 8.675s - 3.658s^2$$

$$\bar{k}_{22} = 3.61 + 15.962s + 5.874s^2 \tag{90}$$

and

$$\bar{c}_{11} = 0.8222 + 13.051s - 0.528s^2$$

$$\bar{c}_{12} = -2.764 + 23.949s - 1.755s^2$$

$$\bar{c}_{21} = -2.764 + 23.949s - 1.755s^2$$

$$\bar{c}_{22} = 4.31 + 43.087s + 6.18s^2 \tag{91}$$

where s is the Summerfield number defined as

$$s = \frac{\mu\omega DL}{W}(\frac{R}{h})^2 \tag{92}$$

where μ, ω and R are lubricant visocity, rotating speed and journal radius, respectively. Therefore, the stiffness and damping matrices of the bearing can be written in the following form;

$$K_b^e = \begin{bmatrix} K_{11} & K_{12} \\ K_{21} & K_{22} \end{bmatrix}; \; C_b^e = \begin{bmatrix} C_{11} & C_{12} \\ C_{21} & C_{22} \end{bmatrix} \tag{93}$$

where the subscripts 1 and 2 correspond to directions x and y, respectively.

III. 6 The system equations of motion

In order to obtain the system equations of motion, the direct stiffness method to assemble the element mass, damping, stiffness and applied force matrices will be used [24]. The system matrices are constructed simply by adding terms from the individual element matrices into their corresponding locations in global matrices. The system equations of the motion for the shaft including rigid disks and bearing system become

$$\boldsymbol{M}\ddot{\boldsymbol{q}} + \boldsymbol{C}\dot{\boldsymbol{q}} + \boldsymbol{K}\boldsymbol{q} = \boldsymbol{f}(t) \tag{94}$$

where

$$\boldsymbol{M} = \boldsymbol{M}^e + \boldsymbol{M}_d{}^e$$

$$\boldsymbol{C} = \boldsymbol{C}^e + \boldsymbol{C}_d{}^e + \boldsymbol{C}_b{}^e$$

$$\boldsymbol{K} = \boldsymbol{K}^e + \boldsymbol{K}_d{}^e + \boldsymbol{K}_b{}^e$$

$$\boldsymbol{f}(t) = \boldsymbol{f}^e(t) + \boldsymbol{f}_d{}^e(t) \tag{95}$$

The system mass, damping, stiffness and applied force matrices are **M**, **C**, **K** and **f**(t), respectively. The generalized coordinates q for the system are

$$\boldsymbol{q} = \boldsymbol{q}_i{}^T = [u_{x1}, u_{y1}, \theta_{x1}, \theta_{y1}, \ldots, u_{x4(m-1)}, u_{y4(m-1)}, \theta_{x4(m-1)}, \theta_{y4(m-1)}]^T \tag{96}$$

$$(i=1,2,\ldots\ldots,4(m-1))$$

where m is the total number of nodes in the system.

In the next chapter, the eigenvalue and stability problem associated with the homogeneous equations of motion combining the rotor and bearing system will be developed. Parametric studies to investigate the effects of various system parameters on the dynamic response using a Newmark-β time integration scheme are presented.

Chapter IV

Parametric Studies

IV. 1 Frequency and stability analysis

The natural frequency of the system at a constant speed of rotation can be obtained from the homogeneous equations of motion. An eigenvalue analysis of the equations of motion can be used to identify the critical speed at which the motion of a rotor will become unbounded.

The complex eigenvalue problem associated with the rotor-bearing system with rigid disks is

$$(M\lambda^2+C\lambda+K)\cdot x=0 \tag{97}$$

where λ is an eigenvalue of the system and x is the corresponding eigenvector. This complex eigenvalue problem can be solved by introducing an additional unknown eigenvector y, resulting in the 2N×2N (N is the degree of freedom) eigensystem,

$$\begin{bmatrix} 0 & I \\ -M^{-1}\cdot K & -M^{-1}\cdot C \end{bmatrix} \begin{bmatrix} x \\ y \end{bmatrix} = \lambda \begin{bmatrix} x \\ y \end{bmatrix} \tag{98}$$

where M, C and K are the mass, damping and stiffness matrices of the complete

system, respectively; and I is an identity matrix. The complex eigenvalues provide complete information about the system frequencies ω and corresponding modal damping ratios β, i.e.

$$\omega = |\lambda|; \quad \beta = -\frac{\Re(\lambda)}{\omega} \tag{99}$$

If the motion of a rotor is stable, the real parts of all the eigenvalues must not be positive which implies that the modal damping ratios are zero or negative. To obtain the speed at which a rotor would become unstable, one can plot the largest real part of the system eigenvalues against the rotating speed. For the rotor-disk-bearing model, one can observe a change from a negative to a positive value at the critical rotation speeds of about 2310 and 104 rpm (see Figure 5).

IV. 2 Parametric studies

In general, the equations of motion of a rotor-bearing system subjected to seismic excitation are quite complex. It is difficult to integrate these equations analytically; therefore a step-by-step approach such as the Newmark-β integration scheme [25] is used.

As an example for seismic analysis, a stable rotor-disk-bearing model is shown in Figure 6. The physical properties of this model are provided in Table 1. The rotor is modelled using 14 finite elements with a total of 60 degrees of freedom. The bearings have stiffness and damping coefficients as given by Lund and Tomsen [23] for elliptical bearings

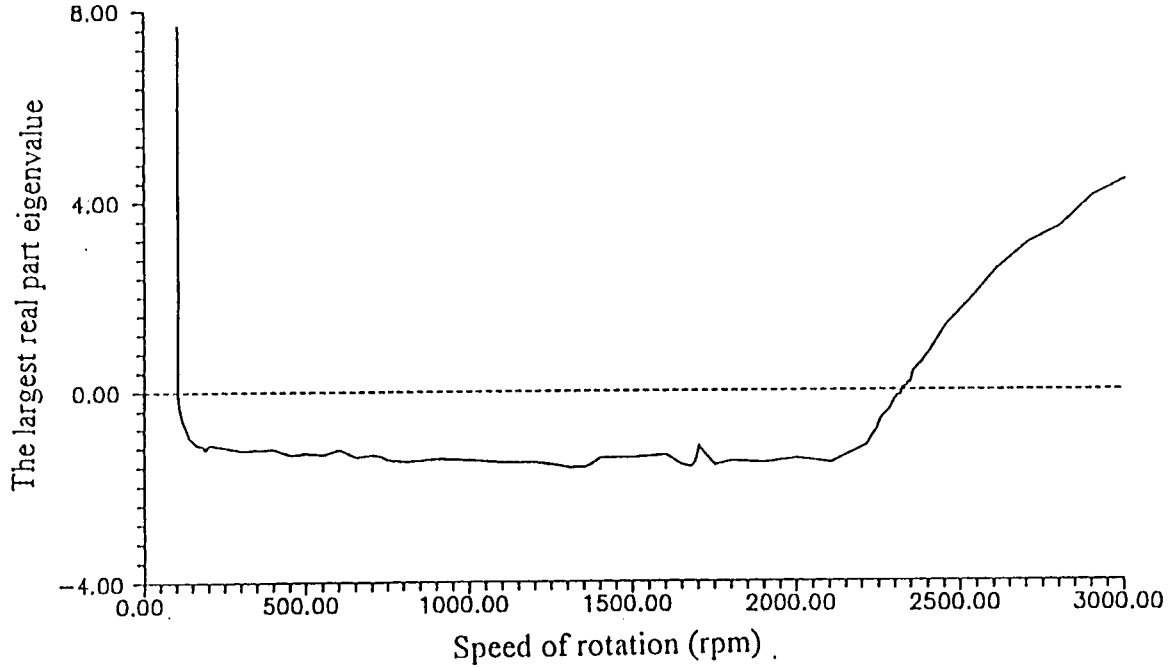

Figure 5. Variation in the largest real part of the system eigenvalues of the rotor with respect to speed of rotation.

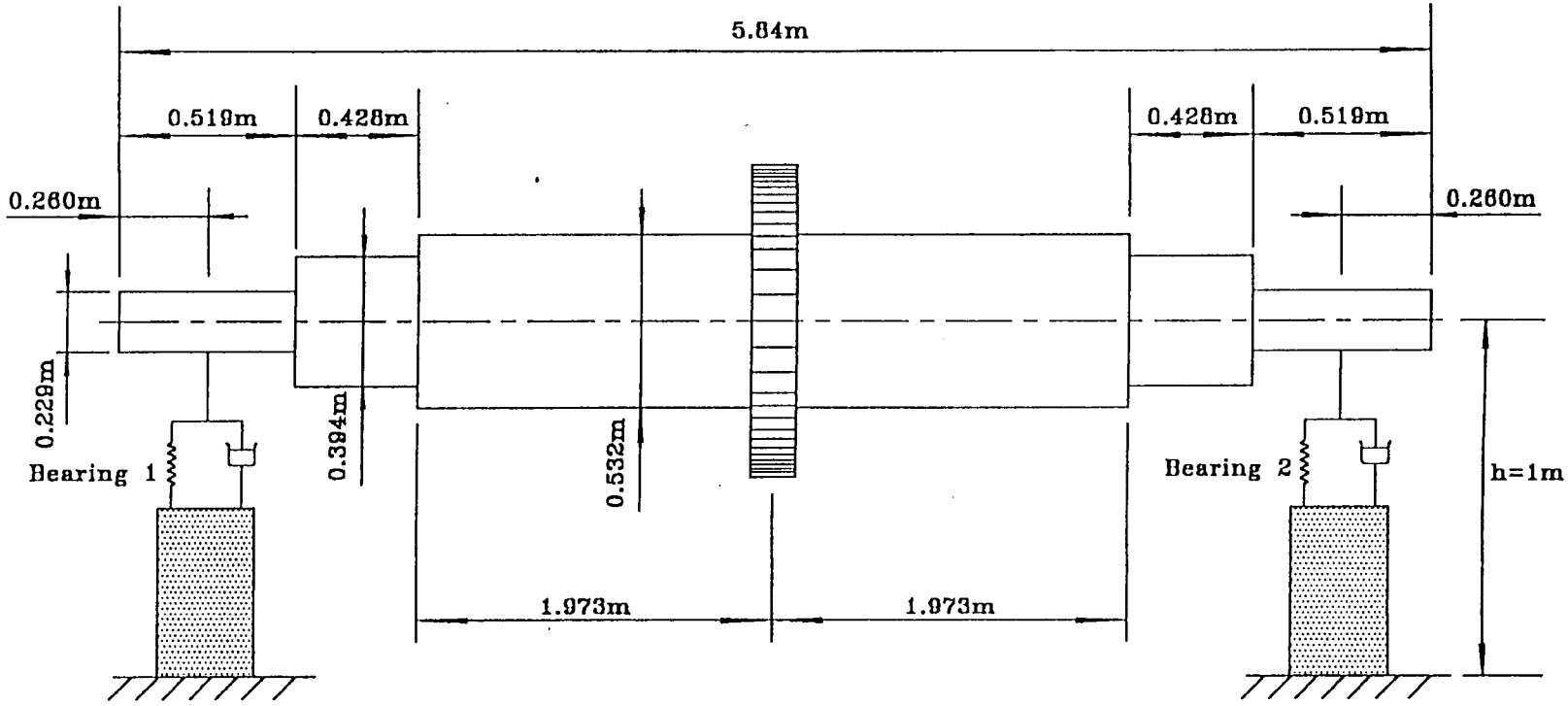

Figure 6. Schematic of a rotor-disk-bearing model considered for seismic response study.

Table 1. Physical and mechanical properties of the rotor machine

Shaft :
Modulus of elasticity, E = 2.078×10^{11} N/m^2
Mass density, ρ = 7806 kg/m^2
Poisson's ratio, ν = 0.3
Revolutions per minute, Ω = 880 rpm

Rotor disk :
Disk mass, m_d = 5670 kg
Transverse moment of inertia, I_x = 3550 kg·m^2
Polar moment of inertia, I_p = 7100 kg·m^2

Bearing system :
Viscosity, μ = 0.14839 N·s/m^2
Diameter of journal, D = 0.229 m
Length of journal, L = 0.229 m
Clearance, C = 3.8×10^{-4}
Weight on bearing, W = 67120 N
L/D ratio = 1.0

Bearing stiffness coefficients (N/m) at operating speed 880 rpm

$K_{xx} = 0.18305\times10^9$ $K_{xy} = 0.37487\times10^9$
$K_{yx} = -0.72481\times10^9$ $K_{yy} = 0.10977\times10^{10}$

Bearing damping coefficients at operating speed (N·s/m)

$C_{xx} = 0.54139\times10^7$ $C_{xy} = 0.17090\times10^7$
$C_{yx} = 0.17090\times10^7$ $C_{yy} = 0.21294\times10^8$

with L/D=1.

The total translational acceleration of the shaft is obtained by adding the approximate results of the Newmark-β approach to the ground acceleration. The relative deformation of the shaft is obtained by considering the rigid body motion induced by the bearing system and the results of the Newmark-β integration scheme. A crude approximation for the maximum normal stress of the shaft can be obtained by the following procedures. Assuming that the bending moment is constant along the shaft, the approximate deformation shape of the shaft is taken as a parabola of the form

$$v(x) = ax^2+bx+c \tag{100}$$

where v(x) is the deformation of the shaft at x position. Since the deformations and location of the ends of the shaft and rigid disk are known, the constants a,b and c can be evaluated. The approximate normal stress σ can be obtained by using the equation M=EIv" and the simple flexure formula σ=Mc/I (where c is the distance from the neutral axis to the extreme fiber).

The maximum relative deformation, absolute translational acceleration and approximate maximum stress of the disk considering shear deformations as well as ignoring shear effects are examined. The seismic response of a rotating machine subjected to different components of the El Centro (1940) earthquake and various speeds of rotation are given in Tables 2-7. Tables 2-7 indicate that the shear term does not have a significant contribution to the maximum responses. Therefore, the shear deformations of the shaft are

neglected in subsequent analysis.

The maximum responses due to different components of Loma Prieta (1989) earthquake and various speeds of rotation are also examined and given in Tables 8-11. Since the vertical component of Loma Prieta (1989) earthquake is significant when compared to the vertical component of the El Centro (1940) record, the maximum responses due to Loma Prieta earthquake is significant then El Centro. Since the governing equations of the motion (29) are coupled, if one or both of the components of earthquake are significant, the responses in both directions will be significant simultaneously. The response time histories of the disk subjected El Centro (1940) and Loma Prieta (1989) earthquakes are shown in Figures 7 and 8.

Effects of shaft flexibility and bearing rigidity on the response of the disk for the rotor-disk-bearing model are given in Tables 12 and 13. From Tables 12 and 13, increasing the flexibility of the shaft as well as the rigidity of the bearing will increase the maximum responses for the particular systems considered.

Consider the rotor-disk-pin model given in Figure 9. The physical properties of the rotor are the same as the rotor-disk-bearing model, except that flexible bearing supports are replaced with pin supports. Damping that was present in the flexible bearing system is absent here, since here is no material damping of the shaft and no damping in the supports. The natural frequency of the system can be obtained from equations (98) and (99). The entire system is undamped, therefore the real parts of the eigenvalues should be zero. This conclusion is indeed substantiated by numerical experiments. The first three natural frequencies of the rotor-disk-pin model are given in Table 14. The response time histories

Table 2. Maximum relative deformation (mm) of the disk considering shear effects for rotor-disk-bearing model subjected to El Centro (1940) earthquake.

operating speed (rpm)	El Centro S00E & vertical components	El Centro S00E component	El Centro vertical component
150	0.203157	0.194874	0.264245
880	0.204163	0.202638	0.189601
1500	0.216140	0.188782	0.190274
2250	0.380290	0.284973	0.215155

Table 3. Maximum relative deformation (mm) of the disk ignoring shear effects for rotor-disk-bearing model subjected to El Centro (1940) earthquake.

operating speed (rpm)	El Centro S00E & vertical components	El Centro S00E component	El Centro vertical component
150	0.225179	0.191825	0.222867
880	0.205061	0.198155	0.177954
1500	0.198774	0.186877	0.181708
2250	0.347791	0.243294	0.204124

Table 4. Maximum absolute acceleration (m/s^2) of the disk considering shear effects for rotor-disk-bearing model subjected to El Centro (1940) earthquake.

operating speed (rpm)	El Centro S00E & vertical components	El Centro S00E component	El Centro vertical component
150	4.77396	4.33634	6.15797
880	4.55867	4.51949	4.24360
1500	4.89356	4.19534	4.25994
2250	8.57095	6.27479	4.80681

Table 5. Maximum absolute acceleration (m/s^2) of the disk ignoring shear effects for rotor-disk-bearing model subjected to El Centro (1940) earthquake.

operating speed (rpm)	El Centro S00E & vertical components	El Centro S00E component	El Centro vertical component
150	5.10355	4.36251	5.21776
880	4.69425	4.51463	4.05918
1500	4.56446	4.24364	4.14968
2250	7.89774	5.45480	4.68362

Table 6. Maximum stress (N/m^2) of the disk considering shear effects for rotor-disk-bearing model subjected to El Centro (1940) earthquake.

operating speed (rpm)	El Centro S00E & vertical components	El Centro S00E component	El Centro vertical component
150	2.57753×10^9	2.47244×10^9	3.35258×10^9
880	2.59029×10^9	2.57094×10^9	2.40554×10^9
1500	2.74225×10^9	2.39515×10^9	2.41408×10^9
2250	4.82488×10^9	3.61556×10^9	2.72975×10^9

Table 7. Maximum stress (N/m^2) of the disk ignoring shear effects for rotor-disk bearing model subjected to El Centro (1940) earthquake.

operating speed (rpm)	El Centro S00E & vertical components	El Centro S00E component	El Centro vertical component
150	2.85693×10^9	2.43376×10^9	2.82760×10^9
880	2.60619×10^9	2.51407×10^9	2.25777×10^9
1500	2.52192×10^9	2.37098×10^9	2.30540×10^9
2250	4.41256×10^9	3.08676×10^9	2.58980×10^9

Table 8. Maximum relative deformation (mm) of the disk ignoring shear effects for rotor-disk-bearing model subjected to Loma Prieta (1989) earthquake.

operating speed (rpm)	Loma Prieta S00E & vertical components	Loma Prieta S00E component	Loma Prieta vertical component
150	0.654945	0.256270	0.651867
880	0.529355	0.255227	0.532416
1500	0.510600	0.279614	0.520532
2250	0.724948	0.394961	0.677929

Table 9. Maximum absolute acceleration (m/s^2) of the disk ignoring shear effects for rotor-disk-bearing model subjected Loma Prieta (1989) earthquake.

operating speed (rpm)	Loma Prieta S00E & vertical components	Loma Prieta S00E component	Loma Prieta vertical component
150	15.1538	5.60715	15.4252
880	12.5824	5.57797	12.6572
1500	12.1266	6.14448	12.3629
2250	16.7221	8.83667	16.0139

Table 10. Maximum relative acceleration (m/s^2) of the disk ignoring shear effects for rotor-disk-bearing model subjected to Loma Prieta (1989) earthquake.

operating speed (rpm)	Loma Prieta S00E & vertical components	Loma Prieta S00E component	Loma Prieta vertical component
150	15.8556	1.88702	15.4014
880	13.3301	2.11672	13.3064
1500	13.4278	2.11363	13.4470
2250	16.5449	5.52459	16.4012

Table 11. Maximum stress (N/m^2) of the disk ignoring shear effects for rotor-disk-bearing model subjected to El Centro (1940) earthquake.

operating speed (rpm)	Loma Prieta S00E & vertical components	Loma Prieta S00E component	Loma Prieta vertical component
150	8.30953×10^9	3.25139×10^9	8.27048×10^9
880	6.71613×10^9	3.23816×10^9	6.75496×10^9
1500	6.47817×10^9	3.54757×10^9	6.60419×10^9
2250	9.19769×10^9	5.01102×10^9	8.60114×10^9

Table 12. Effect of shaft flexibility on response of disk for rotor-disk-bearing model subjected to Loma Prieta (1989) S00E & vertical components.

flexibility	EI	EI	EI/10	EI/10
operating speed (rpm)	relative displacement (mm)	relative acceleration (m/s^2)	relative displacement (mm)	relative acceleration (m/s^2)
150	0.654945	15.8556	135.227	31.8663
880	0.529355	13.3301	111.048	27.0235
1500	0.510600	13.4278	133.456	31.1838
2250	0.724948	16.5449	158.888	37.7953

Table 13. Effect of bearing rigidity on response of disk for rotor-disk-bearing model subjected to Loma Prieta (1989) S00E & vertical components.

rigidity	K	K	K/100	K/100
operating speed (rpm)	relative displacement (mm)	relative acceleration (m/s^2)	relative displacement (mm)	relative acceleration (m/s^2)
150	0.654945	15.8556	0.796388	19.0416
880	0.529355	13.3301	0.635024	14.6453
1500	0.510600	13.4278	0.666907	15.4235
2250	0.724948	16.5449	0.769126	17.1759

Table 14. The first three natural frequencies (Hz) for rotor-disk-pin model

operating speed (rpm)	ω_1	ω_2	ω_3
150	15.4011	15.4945	47.6803
880	15.2074	15.2076	22.3684
1500	14.4186	15.2790	15.8414
2250	9.98505	15.2333	16.1622

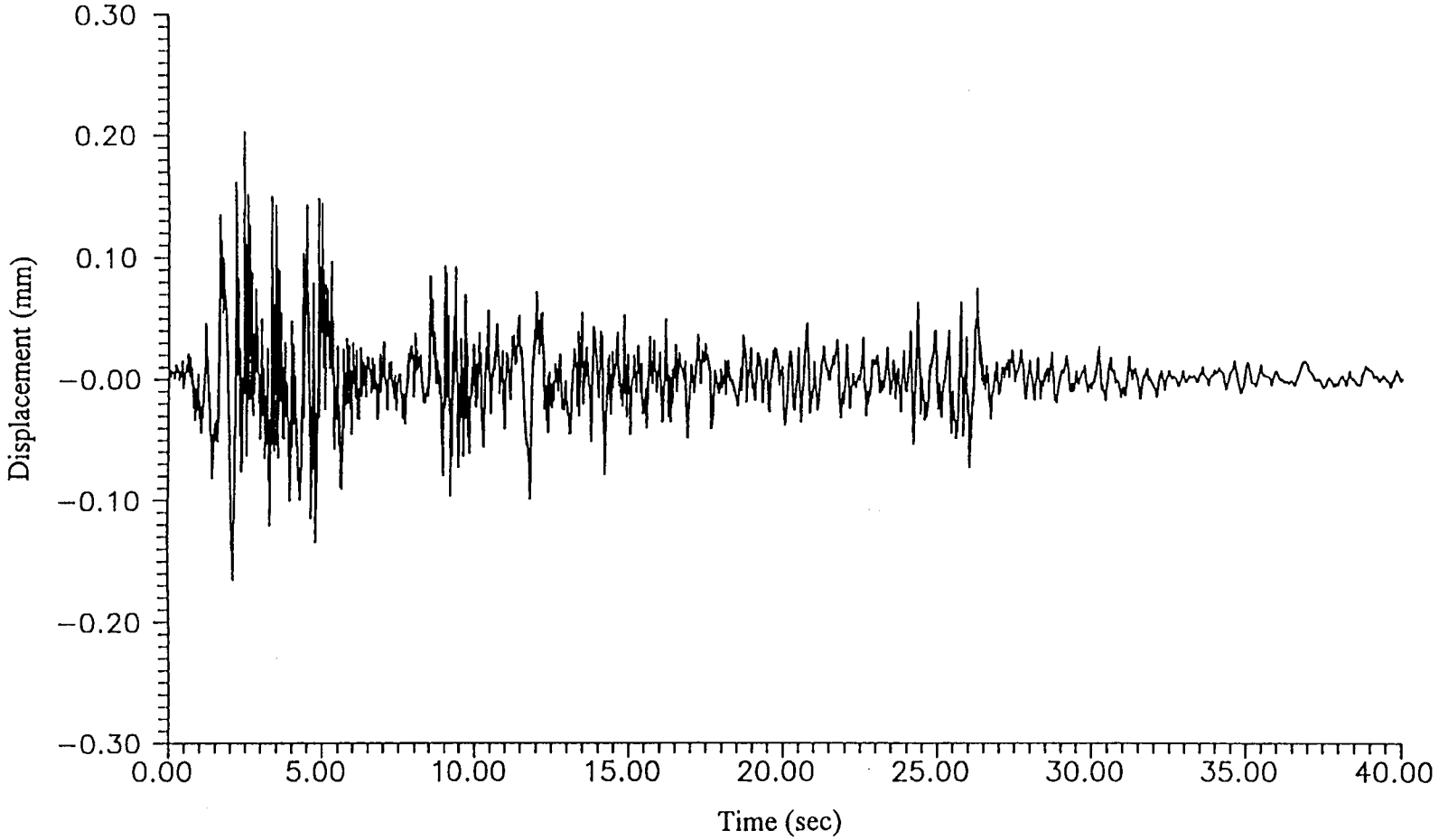

Figure 7. Time history of disk displacement in the X-direction for rotor-disk-bearing model with operation speed 880 (rpm) subjected to El Centro (1940) earthquake.

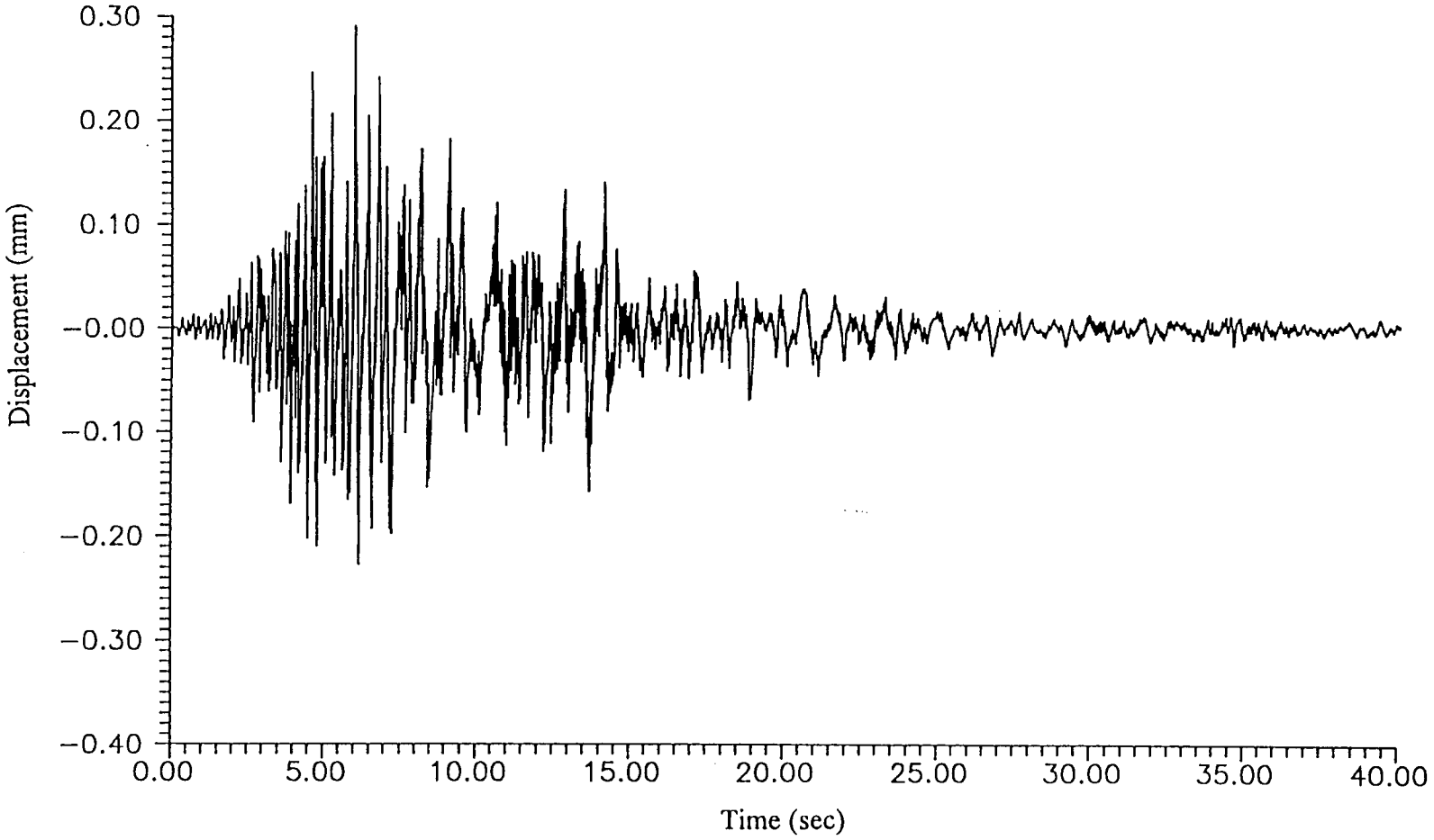

Figure 8. Time history of disk displacement in the X-direction for rotor-disk-bearing model with operation speed 880 (rpm) subjected to Loma Prieta (1989) earthquake.

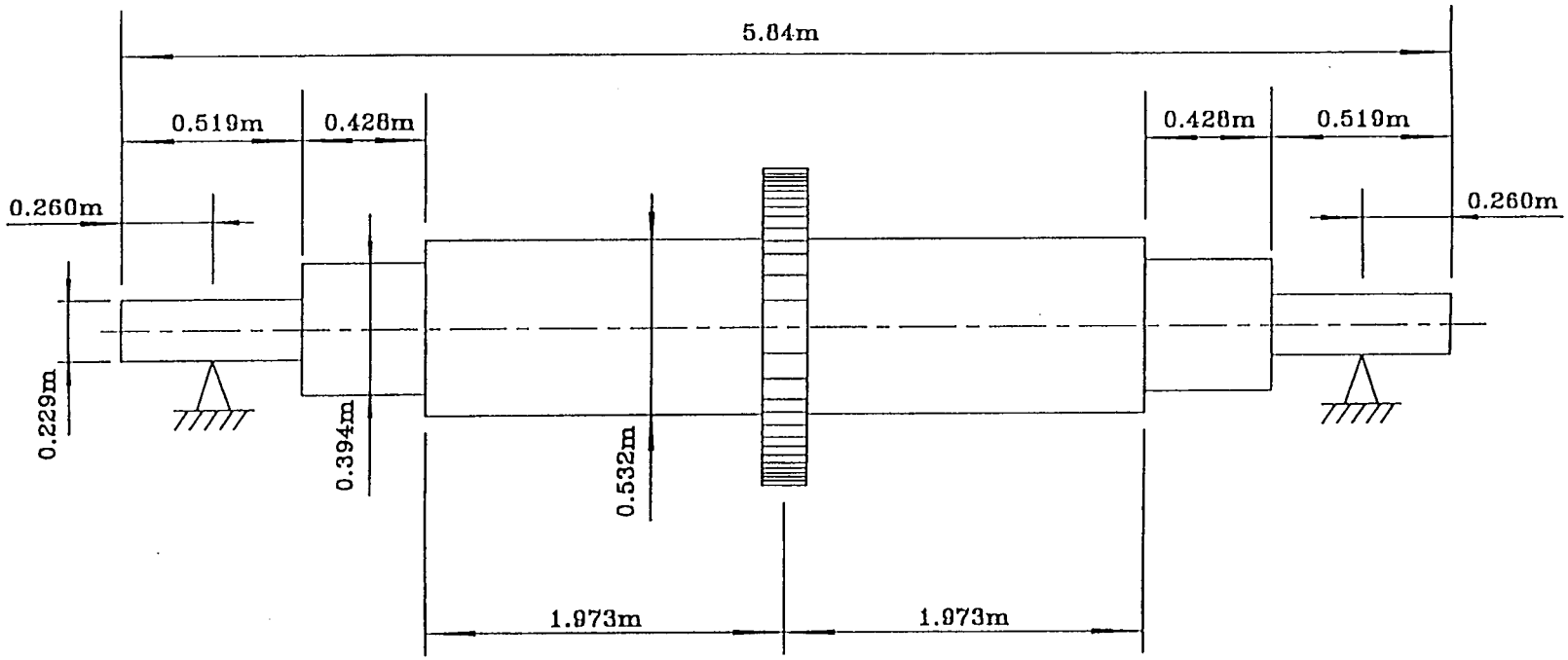

Figure 9. Schematic of a rotor-disk-pin model considered for seismic response study.

of the disk shown in Figure 10 also show that the response of the disk subjected to El Centro (1940) earthquake will not decay when the entire system is undamped.

The maximum responses and approximate normal stress of the rotor-disk-pin model subjected to various components of El Centro (1940) and Loma Prieta (1989) earthquakes are given in Tables 15-17 for both forward and reverse rotations. Comparing Tables 15-17 and Tables 2-7, one can observe that the maximum responses of the disk for the rotor-disk-pin model under forward rotation are larger than those for the rotor-disk-bearing model subjected to the El Centro (1940) earthquake. Tables 15-17 also show the responses of the disk with forward and reverse rotations are slightly different. Referring to equation (51) the term Ω is replaced with $-\Omega$ for the rotating shaft operating in reverse direction. Only slight difference are observed in the responses because the magnitude of this term is small.

For a uniform shaft without disk, the coupled equations for the bending of a rotating shaft for in two directions are given by equations (28) and (29). These two equations can be combined by introducing the symbol q=v+iu, resulting in one complex equation, i.e.

$$\frac{\partial^2}{\partial z^2}[EI\frac{\partial^2 q}{\partial z^2}]-\frac{\partial^2}{\partial z^2}[mk^2(\frac{\partial^2 q}{\partial t^2}-2\Omega i\frac{\partial q}{\partial t})]+m\frac{\partial^2 q}{\partial t^2}=0 \qquad (101)$$

For a rotating uniform shaft supported by pins at both ends (see Figure 11), the eigenfunction of the equation (101) is

Table 15. Maximum absolute deformation (mm) of the disk ignoring shear effects for rotor-disk-pin model subjected to El Centro (1940) earthquake.

operating speed (rpm)	El Centro S00E & vertical components	El Centro S00E component	El Centreo vertical component
150	0.765514	0.528266	0.524406
880	0.777368	0.522127	0.515074
1500	0.808396	0.518949	0.505442
2250	0.841389	0.517235	0.487162
-150	0.759113	0.528271	0.522406
-880	0.737478	0.522154	0.515074
-1500	0.715079	0.518968	0.505442
-2250	0.678080	0.517265	0.487162

Table 16. Maximum absolute acceleration (m/s^2) of the disk ignoring shear effects for rotor-disk-pin model subjected to El Centro (1940) earthquake.

operating speed (rpm)	El Centro S00E & vertical components	El Centro S00E component	El Centreo vertical component
150	17.4589	11.8105	12.1121
880	17.8560	11.7348	11.9226
1500	18.6735	11.7004	11.6983
2250	19.3031	11.6453	11.2719
-150	17.2423	11.8566	12.1121
-880	16.7383	11.8398	11.9226
-1500	16.1857	11.7699	11.6983
-2250	15.3206	11.7491	11.2719

Table 17. Maximum stress (N/m^2) of the disk ignoring shear effects for rotor-disk-pin model subjected to El Centro (1940) earthquake.

operating speed (rpm)	El Centro S00E & vertical components	El Centro S00E component	El Centreo vertical component
150	9.71236×10^9	6.70231×10^9	6.65334×10^9
880	9.86276×10^9	6.62442×10^9	6.53494×10^9
1500	1.02564×10^9	6.58409×10^9	6.41273×10^9
2250	1.06753×10^9	6.56235×10^9	6.18081×10^9
-150	9.63115×10^9	6.70237×10^9	6.65334×10^9
-880	9.35666×10^9	6.62476×10^9	6.53493×10^9
-1500	9.07248×10^9	6.58434×10^9	6.41273×10^9
-2250	8.60306×10^9	6.56276×10^9	6.18081×10^9

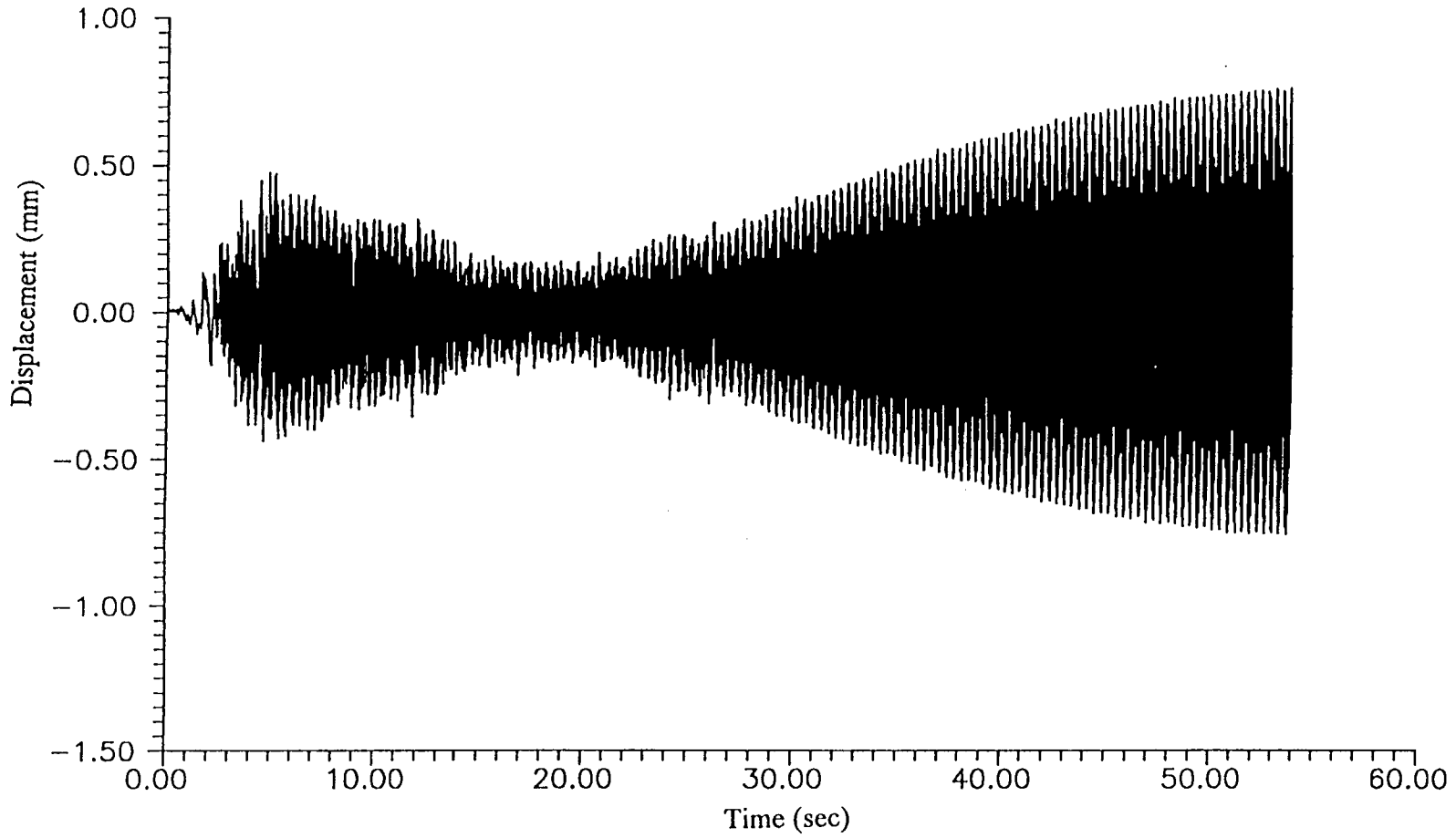

Figure 10. Time history of disk displacement in the X-direction for rotor-disk-pin model with operation speed 880 (rpm) subjected to Loma Prieta (1989) earthquake.

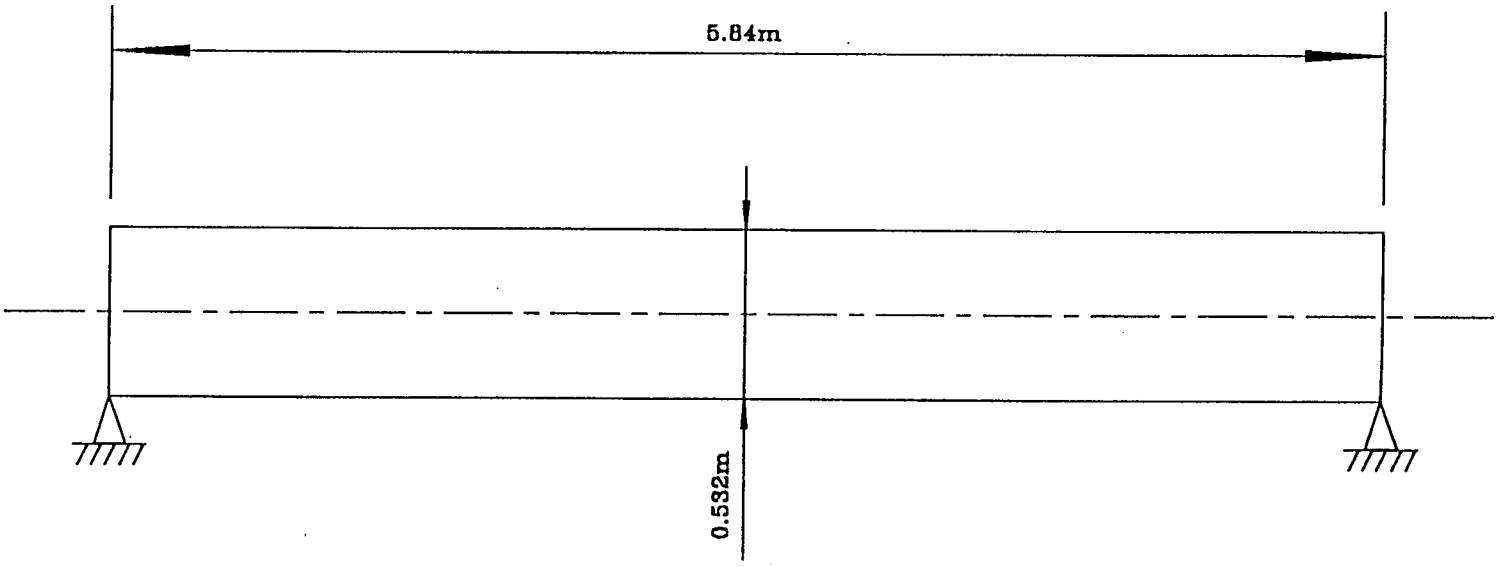

Figure 11. Schematic of a rotor-pin model with uniform cross sectional area considered for seismic response study.

$$q(x,t)=C\sin(\frac{n\pi x}{L})e^{i\lambda t} \quad (n=1,2,3....) \tag{102}$$

where the unknown constant C depends upon the initial conditions The length of the shaft is L and the eigenvalue of the system is λ. For other boundary conditions, the eigenfunctions are offered by Genta [8]. Substitution of equation (102) into expression (100), gives the algebraic equation for the natural frequencies, i.e.

$$(1+\frac{k^2n^2\pi^2}{L^2})\lambda^2-2\Omega\frac{k^2n^2\pi^2}{L^2}\lambda-\frac{EI}{m}\frac{n^4\pi^4}{L^4}=0 \tag{103}$$

Solving equation (103) for a natural frequency λ, results in

$$\lambda=(\frac{k^2n^2\pi^2}{L^2})\frac{\Omega\pm\sqrt{\Omega^2+(1+\frac{k^2n^2\pi^2}{L^2})\frac{EI}{mk^2}}}{1+(\frac{k^2n^2\pi^2}{L^2})} \tag{104}$$

Equation (104) yields two values for λ, one positive and the other negative. Only the positive value for λ is retained, since the negative eigenvalue has no physical significance. In equation (104), forward rotation is given by a positive value for Ω while reverse rotation is given by negative value for Ω. The first three natural frequencies of the uniform shaft without rigid disk for both forward and reverse rotation with the same properties as the previous model (see Table 1) but replacing the flexible bearings with pin supports at

the end are given in Table 18.

In particular, when the speed of rotation is equal to the natural frequency of the system, i.e. when $\lambda=\Omega$, the equation for the determination of critical speeds for forward rotation is

$$(1-\frac{k^2n^2\pi^2}{L^2})\Omega^2-\frac{EIn^4\pi^4}{mL^4}=0 \tag{105}$$

Therefore, the critical speeds Ω_{cf} of forward rotation can be obtained by solving equation (105), i.e.

$$\Omega_{cf}=\frac{n^2\pi^2}{L^2}\frac{\sqrt{\frac{EI}{m}}}{\sqrt{1-\frac{k^2n^2\pi^2}{L^2}}} \tag{106}$$

Substituting $\lambda=-\Omega$ into equation (105), an equation to determine the critical speeds of reverse rotation is obtained, i.e.

$$(1+\frac{3k^2n^2\pi^2}{L^2})\Omega^2-\frac{EIn^4\pi^4}{mL^4}=0 \tag{107}$$

Therefore, the critical speeds Ω_{cr} of reverse rotation can be obtained by solving equation (107), i.e.

Table 18. The first three natural frequencies (Hz) for the uniform shaft without rigid disk and pin supports at the two ends.

operating speed (rpm)	ω_1	ω_2	ω_3
150	198.102	786.424	1747.68
880	198.492	787.959	1751.05
1500	198.823	789.265	1753.91
2250	199.225	790.848	1757.39
-150	197.942	785.794	1746.29
-880	197.553	784.263	1742.93
-1500	197.224	782.965	1740.08
-2250	196.826	781.398	1736.64

$$\Omega_{cr} = \frac{n^2\pi^2}{L^2} \frac{\sqrt{\frac{EI}{m}}}{\sqrt{1+\frac{3k^2n^2\pi^2}{L^2}}} \tag{108}$$

Equation (106) shows that for a particular value of the ratio k/L, the value of Ω_{cf} becomes imaginary when n is sufficiently large, indicating, that there will be no critical speeds in this instance. However, for n=1, the expression in the denominator of equation (106) can be negative when the ratio of the length of the shaft L to the radius of gyration of the cross section k is less than π (i.e. $k/L < \pi$). In this instance as well there are no critical speeds of forward rotation. From equation (108), it can be seen that there is always an infinite number of critical speeds of reverse rotation.

For a particular value of n, the natural frequency λ can be determined as a function of Ω, resulting in a family of curves (see Figure 12). In this figure, the critical speeds of forward and reverse rotation are determined by the intersection of the individual curves with the lines $\lambda=\Omega$ and $\lambda=-\Omega$.

Effect of shaft flexibility for the natural frequency and critical speeds are also examined and given in Table 19 and Figure 13. From Table 19 and Figure 13, one can readily observe that the natural frequencies and critical speeds for the forward and reverse rotations have significant differences when the shaft becomes flexible. Conversely, the natural frequencies and critical speeds for the forward and reverse rotations have no significant differences when the shaft becomes more stiff.

Table 19. The first three natural frequencies (Hz) for the uniform shaft without rigid disk and pin supports at the two ends when the shaft becomes flexible ($EI/10^6$).

operating speed (rpm)	ω_1	ω_2	ω_3
150	0.71124	2.82077	6.25897
880	1.25144	4.94553	10.9100
1500	1.81508	7.16272	15.7643
2250	2.55221	10.0640	22.1220
-150	0.55133	2.19077	4.87614
-880	0.31334	1.24955	2.79739
-1500	0.21604	0.86276	1.93599
-2250	0.15364	0.61404	1.37960

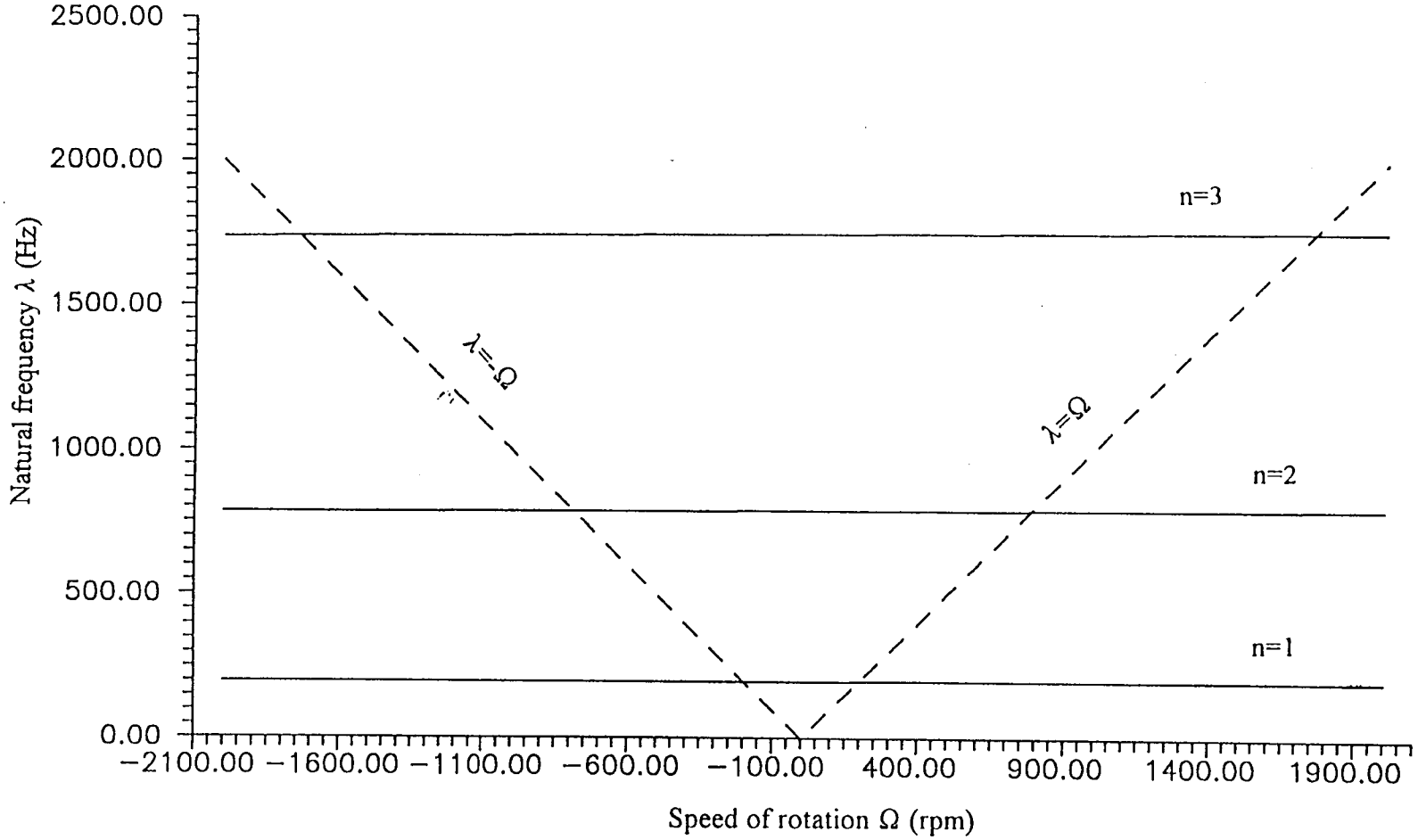

Figure 12. The natural frequency λ of the stiff shaft with respect to speed of rotation Ω for a particular value of n.

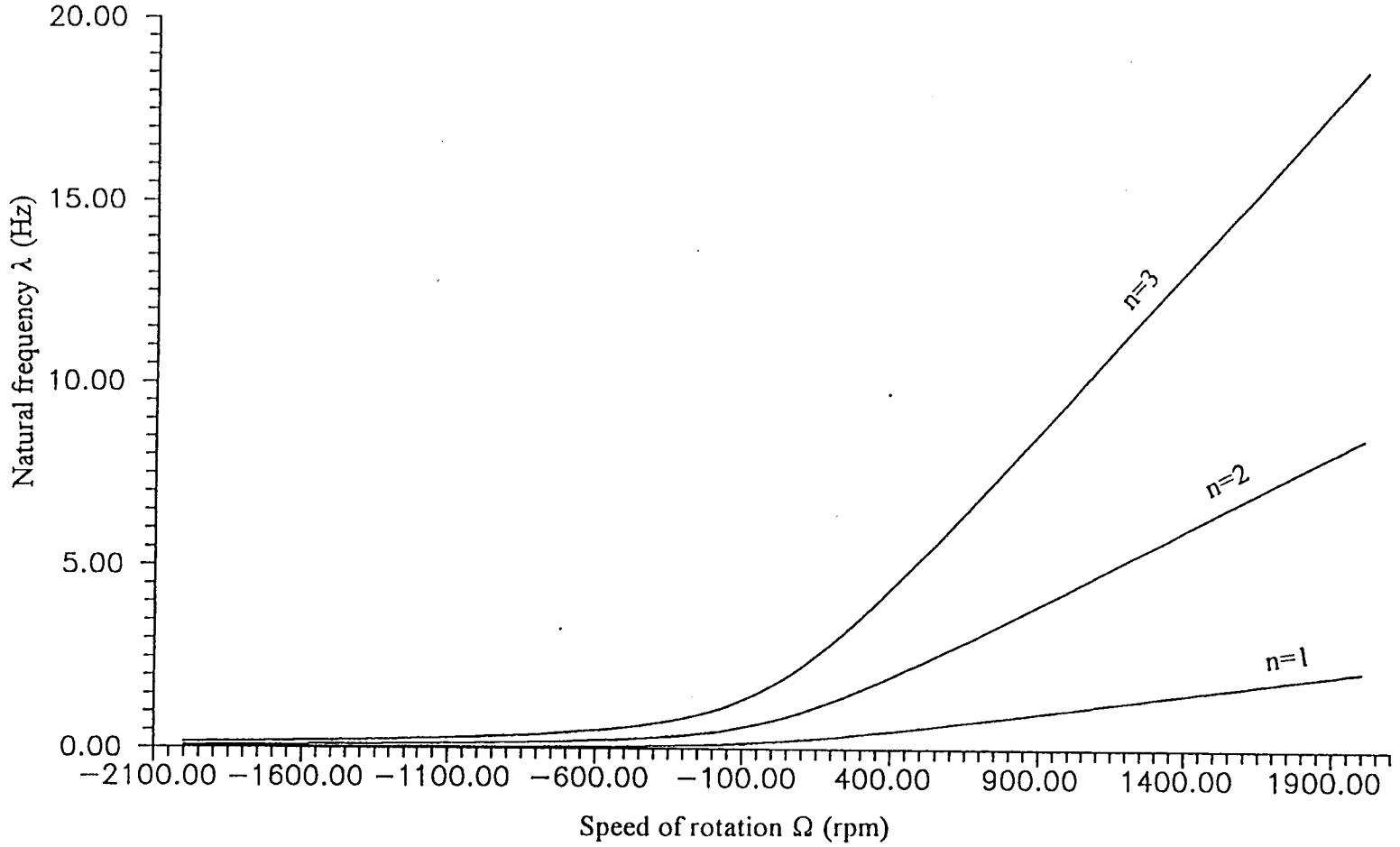

Figure 13. The natural frequency λ of the flexible shaft with respect to speed of rotation Ω for a particular value of n.

Chapter V

Summary and Conclusions

In this thesis, the equations of motion of a flexible rotating machine with uniform properties along the length, constant speed of rotation, mounted on rigid supports at the ends are developed using classical dynamics. These governing equations of motion can be reduced to a single algebra equation for the natural frequencies or critical speeds. The general expressions for the natural frequency and critical speed with any boundary condition, speed of rotation, flexibility of the shaft can also be obtained from these governing equations of motion. In addition, the effect of forward and reverse rotation can be investigated. The study indicates that the responses of the rotating machine have no significant differences for either forward or reverse rotation when the shaft of the rotor is stiff. However, the response for forward or reverse rotation differ significantly when the shaft of the rotor becomes flexible.

Rotating machines may have varying properties along the shaft and rigid disks at arbitrary locations on the shaft. In addition the shaft may be mounted on a flexible bearing system that is subjected to random seismic motions. The effects of shear deformations may be important when the shaft is short and stocky. In general, it is not possible to determine the response of such complex systems using classical techniques. The finite element method serves as a convenient technique for analyzing these systems. Finite element equations based on an energy method are developed. A Newmark-β integration scheme is used to determine the response of the shaft when the system is subjected to seismic

excitation.

Stability of a rotor-disk-bearing system is investigated using the finite element method. The instability of this system is primarily caused by the asymmetric stiffness terms of the fluid-film bearings, even though the fluid-film bearing also provides very desirable damping. The coefficients of the bearing stiffness and damping depend on the speed of rotation, which implies a rotating machine will become unstable at certain operating speeds. The real parts of the eigenvalues can help to identify the instability characteristics of the rotating machine. If a rotating machine is stable, the real parts of the eigenvalues of the system must be negative or zero. Conversely, the responses of the rotor machine will become unbounded when the sign of the largest real part of eigenvalue changes from negative to positive.

For the rotor-disk-pin model where material damping is ignored, all of the real parts of the eigenvalues are zero which implies that the modal damping ratios are zero. This indicates that the system is undamped and that the responses of a rotating machine would not decay with time.

The seismic responses of a rotating machine considering and ignoring shear deformations are examined. Negligible differences in response were observed, thus shear effects can be neglected in a seismic response analysis of systems of the type considered herein. The effects of the flexibility of the shaft and the rigidity of the bearing system on the response of the flexible rotating machine are also examined. Numerical results show that, as expected, large responses are obtained when the shaft or bearing system becomes flexible.

Bibliography

1. J. M. Tessarzik, T. Chiang and R. H. Badgley, *The response of rotating machinery to external random vibration,* J. eng. indust. ASME 96, 477-489 (1974).

2. G. J K. Asmis and C. G. Duff, *Seismic design of gyroscopic systems*, ASME paper 78-PVP 44, ASME/CSME press. vess piping conf. Montreal, Canada (1978).

3. G. J. K. Asmis, *Response of rotating machinery subjected to seismic excitation*, Engineering Design for Earthquake Environments, I. Mech. E. Conference Publication 1978-12, London, 1979, pp.215-255.

4. A. P. Villasor, *Seismic analysis of a rotor coolant pump by the response spectrum method*, Nucl. eng. des. 38, 527-542 (1976).

5. A. H. Soni and V. Srinivasan, *Seismic analysis of a gyroscopic mechanical system*, J. vib. acoustics stress reliability des. ASME 105, 449-455 (1983).

6. T. Iwatsubo, I. Kawahar, N. Nakagawa and R. Kowai, *Reliablity design of rotating machine against earthquake excitation*, Bull. Japan soc. mech. eng. 22, 1632-1639 (1979).

7. B. Samali, K. B. Kim and J. N. Yang, *Random vibration of rotating machines under earthquake excitations*, J. eng. mech ASCE 112, 550-565 (1986).

8. G. Genta, *Vibration of structures and mechanics*, Spring-Verlage, New York (1993).

9. H. D. Nelson and J. M. McVaugh, *The dynamics of rotor-bearing systems using finite element*, J. eng. indust. ASME 98, 593-600 (1976).

10. H. D. Nelson, *A finite rotating shaft element using Timoshenko beam theory*, J. mech. des. ASME 102, 793-803 (1980).

11. E. S. Zori and H. d. Nelson, *Finite element simulation of rotor-bearing systems with internal damping*, J. eng. power ASME 99, 77-86 (1977).

12. E. Hashish and T. S. Sankar, *Finite element and model analysis of rotor-bearing system under stochastic loading conditions*, J. vib. acoustics stress reliability des. ASME 106, 81-89 (1984).

13. K. B. Kim, J. N. Yang and Y. K. Lin, *Stochastic response of flexible rotor-*

bearing systems to seismic excitations, prob. eng. mech. 1, 122-130 (1986).

14. V. Srinivasan and A. H. Soni, *Seismic analysis of rotating mechanical systems - a review*, Shock vib. dig. 14(6),13-19 (1982).

15. V. Srinivasan and A. H. Soni, *Seismic analysis of a rotor-bearing system*, Earthquake eng. struct. dyn. 12, 287-311 (1984).

16. L. E. Suarez, M. P. Singh and M. S. Rohanimanesh, *Seismic response of rotating machines*, Earthquake eng. struct. dyn. 21, 21-36 (1992).

17. A. K. Chugh, *Stiffness matrix for a beam element including transverse shear and axial force effects*, International journal for numerical methods in engineering 11, 1681-1697 (1977).

18. T. R. Kane and D. A. Levinson, *Dynamics : Theory and Applications*, McGraw-Hill, New York (1985).

19. F. M. Dimentberg, *Flexural vibrations of rotating shaft*, Butterworths Inc., Washington D. C. (1961).

20. J. B. MArion and S. T. Thornton, *Classical dynamics of particles and systems*, Saunder college publishing, New York (1988).

21. J. N. Reddy, *Finite element method*, McGraw-Hill Inc., New York (1993).

22. J. S. Rao, *Rotor dynamics*, Wiley, New Delhi (1983).

23. L. L. Earles and A. B. Palazzolo, *Hybrid finite element - boundary element simulation of rotating machinery supported on flexible foundation and soil*, Rotating machinery dynamics vol. 2, 371-381 (1987).

24. W. B. Bickford, *A first course in the finite element method*, Richard D. Irwin Inc., Boston (1990).

25. N. M. Newmark, *A method of computation for structure dynamics*, J. eng. mech. div. ASCE 85, No. EM3, 67-94 (1959).

26. J. W. Lund and K. K. Tomsen, *A calculation method and data for the dynamic coefficients of oil-lubricated journal bearings*, in Topics in Fluid Film Bearing and Rotor Bearing System Design and Optimization, ASME, The Design Engineering Conference, Chicago, IL, 1-28 (1978).